Propagator of the Δ resonance and determination of the magnetic moment of the Δ^+ from the $\gamma p \to \gamma\pi^o p$ reaction

A. I. Machavariani[1,2,3] and Amand Faessler[1]
[1]*Institute für Theoretische Physik der Universität Tübingen, D-72076 Tübingen, Germany*
[2]*Joint Institute for Nuclear Research, Dubna, Moscow Region RU-141980, Russia*
[3]*High Energy Physics Institute of Tbilisi State University, University str. 9, Tbilisi 380086, Georgia*
(Received 9 December 2003; revised manuscript received 22 November 2004; published 19 August 2005)

The photon-proton scattering reactions $\gamma p \to \pi^o p$, $\gamma p \to \gamma p$, and $\gamma p \to \gamma\pi^o p$ are investigated in the framework of the three-dimensional time-ordered approach using different models of the on-shell Δ propagators. These Δ propagators are taken from the unitary separable models of the πN elastic-scattering amplitude and from the relativistic Breit-Wigner shape representation of the nonunitary πN amplitude in the tree approach. The numerical calculations are performed with the complete set of the one-particle (π-, ω-, and ρ-meson, nucleon, and Δ) exchange diagrams. It is found that the numerical calculations of the above reactions in the Δ-resonance region are very sensitive to the model of the Δ propagator. This sensitivity is explained by the difference between the input πN elastic-scattering observables used for the construction of the Δ propagator. It is shown, that after additional approximation our calculations reproduce the tree-level model calculations with the Breit-Wigner shape Δ propagator. This model is in good agreement with the $\gamma p \to \pi^{o\prime} p'$ reaction and with the preliminary data for the $\gamma p \to \gamma'\pi^{o\prime} p'$ reaction. Conversely, it is demonstrated, that the relativistic Breit-Wigner shape Δ propagators, obtained from the nonunitary πN amplitudes in the tree approximation, is inconsistent to apply for reproduction of the γp scattering observables because they do not describe the πN scattering data in the Δ resonance region. It is emphasized, that to extract the magnitude of the Δ^+ magnetic moment from the cross sections of the $\gamma p \to \gamma'\pi' N'$ reaction it is necessary to fix the form of the Δ propagator based on the unified description of the two body $\pi p \to \pi N$, $\gamma p \to \pi N$ basic channels together with the essential $\gamma p \to \pi\pi N$ and $\gamma p \to \gamma p$ reactions.

DOI: 10.1103/PhysRevC.72.024002 PACS number(s): 13.40.−f, 13.60.−r, 13.75.−n

I. INTRODUCTION

This article concerns an investigation of the role of the propagator of the Δ resonance in the $\gamma p \to \pi N$, $\gamma p \to \gamma p$, and $\gamma p \to \gamma\pi^o p$ reactions and an estimation of the possibility to extract the value of the magnetic dipole moment of the $\Delta^+(1232)$ resonance from the $\gamma p \to \gamma\pi^o p$ reaction. Interest in investigation of reactions with the three-body final $\gamma\pi p$ states originated by the proposal to determine the magnetic moment of the Δ^{++} resonance in the $\pi^+ p \to \gamma'\pi^{+\prime} p'$ reaction [1]. The basic idea of this investigation is to separate the contribution of the $\Delta \to \gamma'\Delta'$ vertex function, which, in analogy to the $N - \gamma' N'$ vertex, contains at threshold the magnitude of the Δ magnetic moment. The first numerical estimation of the contribution of the $\Delta^+ \to \gamma'\Delta^{+\prime}$ vertex function in the $\gamma p \to \gamma'\pi^{o\prime} p'$ reaction was done in Refs. [2–4]. The first data about the $\gamma p \to \gamma'\pi^{o\prime} p'$ reaction were obtained in a recent experiment by the A2/TAPS collaboration at Mainz Microtron (MAMI) [5] and future experimental investigations of this reaction are planed by using the Crystal Ball detector at MAMI [6].

The investigation of the coupled $\pi N - NN - \pi NN$ scattering reactions based on the separable model of the two-body amplitudes [7] has demonstrated that the difference between the corresponding cross sections calculated with the different Δ propagators is not larger as ∼20%. In contrary to this the high sensitivity of the $\gamma p - \pi N$ and $\gamma p - \gamma p$ scattering amplitudes on the off shell behavior of the Δ propagators was underlined in Refs. [8,9]. Therefore the problem of sensitivity of the γp scattering reactions on the choice of the separable model of the Δ propagators appears.

In our previous article [10] we have obtained the three-body relativistic equations for the coupled $\pi N \Longleftrightarrow \gamma N \Longleftrightarrow \pi\pi N \Longleftrightarrow \gamma\pi N$ reactions in the framework of the three-dimensional time-ordered field theoretical approach. This formulation enables us to avoid a number of approximations that are usually done in the other field-theoretical equations. For instance, this formulation is free from the ambiguities that arise in the Bethe-Salpeter equations by the three-dimensional reduction and the effective potentials of the suggested equation are constructed from the one-variable vertices with two on mass-shell particles. Moreover in the Coulomb gauge any term of the effective potential is invariant under the gauge transformations. In the present article we restrict our calculation by the Born approximation and we compare our results with the recent appropriate calculations performed in the tree approximation.

In this article we consider also the explicit relation between the Δ resonance part of the πN Green function in the separable representation and the microscopic Δ resonance propagator in the Rarita-Schwinger form. This allows us to examine and to analyze the dependence of the cross sections of the $\gamma p \to \gamma' p'$, $\gamma p \to \pi^o p$, and $\gamma p \to \gamma\pi^o p$ reactions in the different models of the Δ propagators.

The article contains seven sections. In Sec. II the construction of the amplitude of the $\gamma p \to \gamma'\pi' N'$ reaction in the old fashioned perturbation theory [or in the spectral decomposition method over the asymptotic (Fock space) states] is briefly considered and the complete set of time-ordered diagrams is presented. The main advantage of this formulation is that in the input vertex functions nucleons and Δ's are on mass shell. Unlike in our recent three-body equations for the description of the $\gamma p \Longleftrightarrow \pi N \Longleftrightarrow \pi\pi N \Longleftrightarrow \gamma\pi N$ reactions [10], in this work we have extracted the three particles γ, γ', π' from the asymptotic states of the S-matrix of the $\gamma p \to \gamma'\pi' N'$ reaction. We have further restricted our calculation to the Born approximation as it is usually assumed in the models based on the effective Lagrangian method. Section III deals with the application of the Coulomb gauge to our three-dimensional time-ordered formulation. It is shown, that this gauge insures the validity of the current conservation condition for every diagram if the input vertex functions are gauge invariant. Section IV is devoted to the problem of the construction of the on-mass shell Δ propagator from the intermediate πN interactions in the old perturbation theory. Section V deals with a generalization of the separable model of the resonance πN t matrix for the case of the spin-3/2 particle propagators. In Sec. VI the numerical results of our calculations are given. The conclusions are presented in Sec. VII. In the appendix all of the input vertices with the corresponding parametrization are listed.

II. ONE-PARTICLE EXCHANGE FIELD-THEORETICAL MODEL OF THE $\gamma N \to \gamma'\pi' N'$ REACTIONS

In the multichannel formulation [10] the interesting $\Delta \to \Delta'\gamma'$ vertex function arise in the perturbation series in the intermediate stage. In this article we use more transparent way of representation of the Born terms for the $\gamma p \to \gamma'\pi^{o\prime}p'$ amplitude with the all possible one-particle exchange contributions. In particular, unlike to Ref. [10] starting from the standard reduction formulas [11,12], we extract three off-mass shell particles: initial and final photons and the final pion. Therefore the $\gamma N \to \gamma'\pi' N'$ scattering amplitude takes the following form:

$$\begin{aligned}\mathcal{T}_{\mu\nu} &= \langle \text{out}; \mathbf{p}'_N \mathbf{p}'_\pi \mathbf{k}'_\gamma \mu | J_\nu(0) | \mathbf{p}_N\rangle \\ &= \sum_{\text{permutation}\,\gamma\gamma'\pi'} \int d^4x \int d^4y e^{ik'_\gamma x + ip'_\pi y} \\ &\quad \times \langle \mathbf{p}'_N | J_\mu(x)\theta(x_o - y_o) j_{\pi'}(y)\theta(y_o) J_\nu(0)|\mathbf{p}_N\rangle \\ &\quad + \text{equal time commutators,}\end{aligned} \tag{1}$$

where $k_\mu, \epsilon^\nu(\mathbf{k},\lambda)$ and $k'_\mu, \epsilon^\nu(\mathbf{k}',\lambda')$ indicate the four-momentum and polarization vector of the initial and the emitted photon, $p_N = (E_{\mathbf{p_N}}, \mathbf{p_N})$, $p'_N = (E_{\mathbf{p'_N}}, \mathbf{p'_N})$, and $p'_\pi = (E_{\mathbf{p}'_\pi}, \mathbf{p}'_\pi)$ denote the on-mass shell four-momentum of nucleons and the pion in the initial and final states and

$$\left(\frac{\partial^2}{\partial x_\nu \partial x^\nu} + m_\pi^2\right)\Phi_\pi(x) = j_\pi(x), \quad \frac{\partial^2}{\partial x_\nu \partial x^\nu} A_\mu(x) = J_\mu(x).$$

Substituting the completeness condition $\sum_n |n; in\rangle \langle in; n| = \mathbf{1}$ in Eq. (1), we get after integration over x and y

$$\begin{aligned}\mathcal{T}_{\mu\nu} = (2\pi)^6 &\sum_{\text{permutation}\,\gamma\gamma'\pi'} \left\{ \sum_{n,m} \langle \mathbf{p}'_N | J_\mu(0)| m; in\rangle \right. \\ &\times \frac{\delta(\mathbf{k}'_\gamma + \mathbf{p}'_\mathbf{N} - \mathbf{P_m})}{E_{k'_\gamma} + E_{p'_N} - P^o_m + io} \langle in; m | j_{\pi'}(0)| n; in\rangle \\ &\times \left. \frac{\delta(\mathbf{k}'_\gamma + \mathbf{p}'_\mathbf{N} + \mathbf{p}'_\pi - \mathbf{P_n})}{E_{k'_\gamma} + E_{p'_N} + E_{p'_\pi} - P^o_n + io} \langle in; n | J_\nu(0)|\mathbf{p}_N\rangle \right\} \\ &+ \text{equal time commutators,}\end{aligned} \tag{2}$$

where $P_n = (P^o_n, \mathbf{P}_n)$ denotes the total four-momentum of the n-particle intermediate states $|n; in\rangle$ $P_n = (P^o_n, \mathbf{P}_n) = \sum_i^n p_i$. The diagrammatic representation of Eq. (2) without equal-time commutators is given in Fig. 1. There only on-mass shell particle exchange propagators with the total four-momentum $P_n = (P^o_n, \mathbf{P}_n) = \sum_i^n (\sqrt{m_i^2 + \mathbf{p}_i^2}, \mathbf{p}_i)$ shown in the intermediate states. Therefore the three-dimensional diagrams in Fig. 1 are not Feynman diagrams. In the time-ordered diagram 1a firstly the incident photon is absorbed on the incoming nucleon and the intermediate on-mass shell state $n = N, \pi N, \ldots$ is arised. Afterwards this intermediate n-particle state emits the final photon and transforms into other set of the on-mass shell m-particle states. At last this m-particle state transforms in the final pion (π') and nucleon (N') state. This diagram with the intermediate πN, $\pi' N'$, or Δ, Δ' states contains the sought $\Delta \to \gamma'\Delta'$ vertex function. The diagram **b** in the Fig. 1 is obtained after permutation of the final photon and pion (i.e., first the final pion is emitted and afterwards the final photon is radiated). This permutation procedure is denoted by the operator $\mathcal{P}_{ab}$ of particles a and b in Eq. (2). In diagrams **c**, **d**, **e**, and **f** of Fig. 1 all other possible permutations of γ, γ', and π' of digram **a** in Fig. 1 are given. This basic diagram is referred as the s-channel diagram [s].

In the processes depicted in the Fig. 1, the initial nucleon is absorbed first and after some intermediate transformation the final nucleon is emitted as the last. After transposition of the N and N' states we get $\overline{s}$-channel diagrams with the antiparticle $\overline{s}, \overline{m}$, intermediate states.

Other source for the construction of the coupled diagrams is the cluster decomposition procedure [22,13], which allows us to take into account other chronological sequences of the external particle emission and absorption. This procedure is well described in Ref. [22,13] and in our previous article. Therefore here we present only eight diagrams in Figs. 2**B–I** that appear after cluster decomposition shown in diagram **a** in Fig. 1.

The second part of Eq. (1) or Eq. (2) with the equal-time commutators have the following form:

$$\begin{aligned}\mathcal{Y} &\equiv \text{equal time commutators} \\ &= \sum_{\text{permutation}\,\gamma\gamma'\pi'} \int d^4x \int dy_o e^{ik'_\gamma x} \langle \mathbf{p}'_N | J_\mu(x)\theta \\ &\quad \times (x_o - y_o)\delta(y_o)[a_{p_{\pi'}}(y_o), J_\nu(0)]|\mathbf{p}_N\rangle\end{aligned} \tag{3a}$$

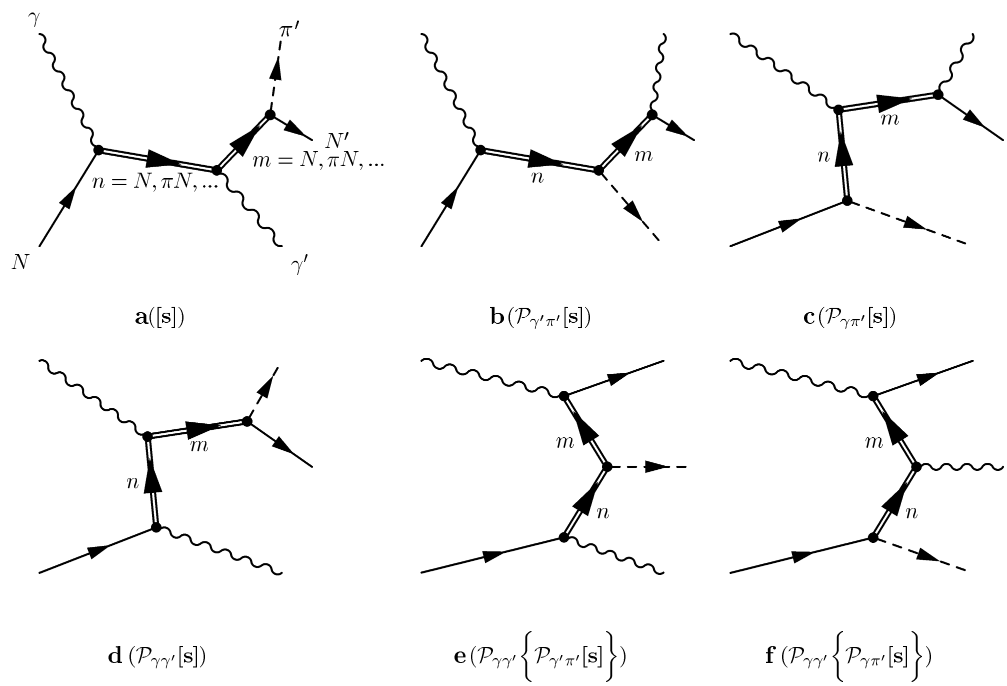

FIG. 1. Diagrammatic representation of the first part of the scattering amplitude for the $\gamma N \to \gamma'\pi' N'$ reaction in the Eq. (2) with the complete set intermediate on mass shell states $|m; \mathrm{in}\rangle$ and $|n; \mathrm{in}\rangle$ with $m, n = N, \pi N, \ldots$. These diagrams correspond to all possible permutations of the γ, γ', and π' source operators in Eq. (2).

or

$$\mathcal{Y} = \sum_{\text{permutation } \gamma\gamma'\pi'} \left\{ \sum_{n=N'',\pi''N'',\ldots} \langle \mathbf{p}'_N | J_\mu(x) | n; in \rangle \times \frac{(2\pi)^3 \delta(\mathbf{k}'_\gamma + \mathbf{p}'_\mathbf{N} - \mathbf{P}_\mathbf{n})}{E_{k'_\gamma} + E_{p'_N} - P^o_n + io} \langle in; n | [a_{p_{\pi'}}(0), J_\nu(0)] | \mathbf{p}_N \rangle \right\}, \tag{3b}$$

where the operator

$$a_{p_{\pi'}}(y_o) = i \int d^3\mathbf{y} \exp(i p_{\pi'} y) \overleftrightarrow{\partial_{y_o}} \Phi_{\pi'}(y) \tag{4}$$

transforms into the pion annihilation operator in the asymptotic region $y_0 \to \infty$.

The diagrammatic representation of Eq. (3b) is given in Fig. 3, where the dashed circle denotes the equal time commutator $\mathcal{Y}_{ab}$ between the operators of the particle a and of the source operator of the particle b. In diagrams **a**, **b**, and **c** the equal-time commutators comes first and afterwards the final nucleon is emitted. In diagrams **c**, **d**, and **e** the target nucleon is absorbed first and after this appears the term with the equal time commutator. To take into account the connected parts of the transition amplitudes in diagrams **i** and **e** we must carry out the cluster decomposition of Eq. (3b). After this procedure every diagram in Fig. 3 produces three additional skeleton diagrams. The three additional diagrams, which appear after the cluster decomposition of the diagram in Fig. 3(a), are given in Fig. 4.

The exact form of the equal time commutator is depending on the choice of a Lagrangian model. For example, if we take the interaction Lagrangian with intermediate vector $V = \rho, \omega$ mesons

$$\mathcal{L}_{\text{int}} = g_V / m_\pi \epsilon_{\mu\nu\gamma\delta} A^\mu(x) \partial^\nu \Phi_\pi(x) \partial^\gamma V^\delta(x), \tag{5}$$

where the photon source operator is $J_\mu(x) = g_V / m_\pi \epsilon_{\mu\nu\gamma\delta} \partial^\nu \Phi_\pi(x) \partial^\gamma V^\delta(x)$, then for the equal time commutator we get

$$\begin{aligned} &\langle \mathbf{p}'_N | \left[J^V{}_\mu(x), a_{\mathbf{p}'\pi}(x_o) \right] \theta(x_o) J_\nu(0) | \mathbf{p}_N \rangle \\ &\quad \Longrightarrow \text{the one nucleon exchange part} \\ &\quad = -i(2\pi)^3 \sum_{\mathbf{p}''_N} \frac{g_V}{m_\pi} \epsilon_{\mu\beta\gamma\delta} p'^{\,\beta}_\pi (p'_N - p''_N)^\gamma \\ &\qquad \times \langle \mathbf{p}'_N | V^\delta(0) | \mathbf{p}''_N \rangle \frac{\delta(\mathbf{k}'_\gamma + \mathbf{p}'_\mathbf{N} - \mathbf{p}''_\mathbf{N})}{E_{k'_\gamma} + E_{p'_N} - E_{p''_N}} \langle \mathbf{p}''_N | J_\nu(0) | \mathbf{p}_N \rangle, \end{aligned} \tag{6}$$

where

$$\langle \mathbf{p}'_N | V^\delta(0) | \mathbf{p}''_N \rangle = \frac{-g^{\delta\sigma} + p_V{}^\delta p_V{}^\sigma / t}{m_V^2 - t} \langle \mathbf{p}'_N | j^V{}_\sigma(0) | \mathbf{p}''_N \rangle$$

and m_V is the V-meson mass, $p_V{}^\mu = p'_N{}^\mu - p_N{}^\mu$, $t = p_V{}^\mu p_{V\mu}$ and the V-meson source operator is $(\partial^2{}_x + m_V^2)$ $V_\mu(x) = j^V_\mu(x)$. An illustration of Eq. (6) is given in Fig. 5. It is important to note that the $\gamma\pi \to V = \rho, \omega$ vertex function in Eq. (6) and in Fig. 5 is in the tree representation.

In Refs. [20,23] it was shown, that the equal time commutators reproduces exactly the off-mass shell σ, ρ, and ω-meson-exchange diagrams for the πN and NN interactions. In addition to Eq. (3b) contain the contact (overlapping) terms. For instance, if we take Lagrangian $\mathcal{L}_I = e^2 A_\mu A^\mu \phi^2_\pi(x)$,

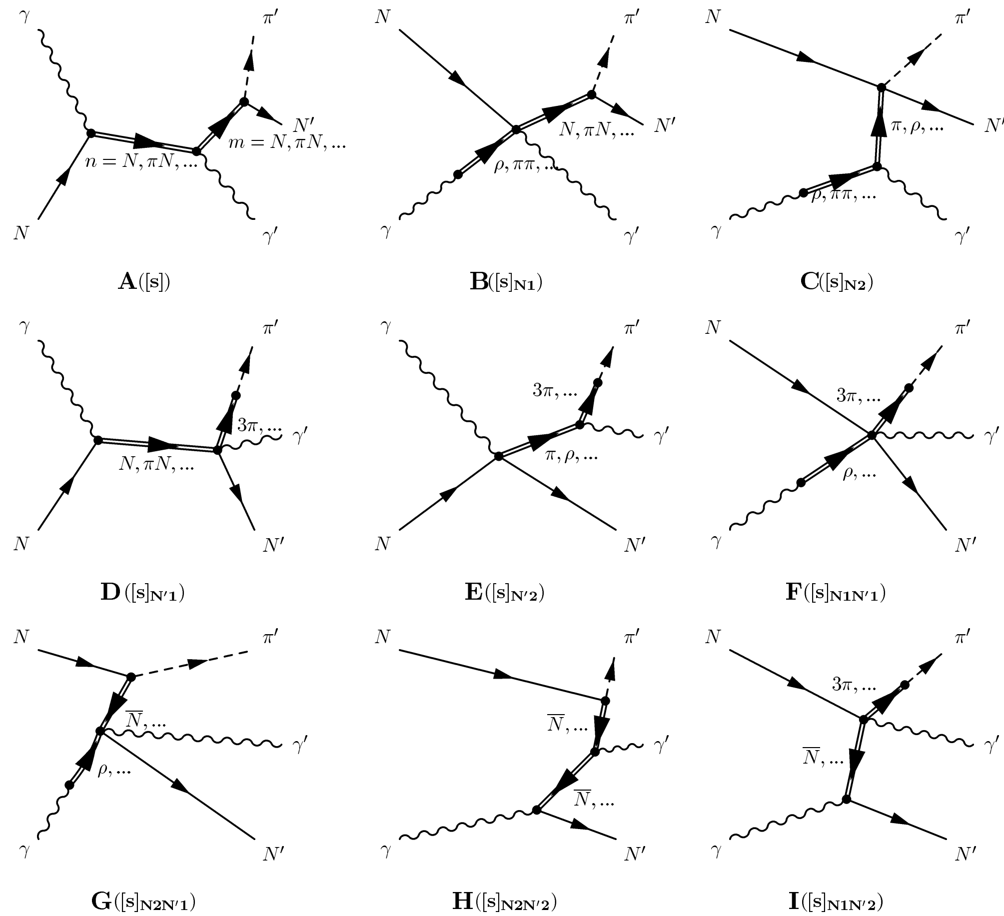

FIG. 2. Skeleton diagrams that appear after the cluster decomposition of the three-dimensional diagram **A** which is the s-channel diagram **a** in Fig. 1. Diagram **B** corresponds to the transposition of the initial nucleon N from the first $\gamma N \to n$ vertex function in **A** to the second vertex $n\gamma' \to m$. This transposition is denoted as $N1$. **C** corresponds to the transposition of N to the third $m \to \pi' N'$ vertex in **A** and it is denoted as $N2$. **D** and **E** are result of the transposition of the final nucleon N' into the second and into the first vertex functions of **A**. These transpositions of N' are denoted as $N'1$ and $N'2$ correspondingly. **E**, **F**, **G**, **H**, and **I** are generated after simultaneous transposition of N and N' with the one or two positions into the vertex functions of the initial **A**.

then the equal time commutator generates the contact term $4ie^2\langle \text{out}; \mathbf{p}'_N \mathbf{k}'_\gamma | A_\nu(0)\phi_\pi(0)|\mathbf{p}'_N\rangle$, which cannot be reduced to the particle exchange diagrams. The amplitudes of the low-energy NN and πN scattering reactions were calculated in the framework of the one off- and on-mass shell-particle-exchange interactions together with the contact (overlapping) terms in our previous articles [20,23]. In Refs. [20,21,24] was shown that in the quantum field theories with quark-gluon degrees of freedom the form of the scattering Eq. (2) does not change and all effects of the pure quark-gluon exchange are contained in the equal time commutators.

Diagrams in Figs. 1 and 3 after corresponding cluster decomposition reproduce the complete set of the one-particle-exchange diagrams in Fig. 11 for the $\gamma p \to \gamma' \pi^{o\prime} N'$ reaction without the antinucleon degrees of freedom.

III. COULOMB GAUGE: CURRENT CONSERVATION CONDITION AND GAUGE INVARIANCE

In the present three-dimensional time-ordered formulation that is often called "old-fashion Perturbation theory," the Coulomb gauge is the natural way to exclude the nonphysical degrees of freedom of photons and to ensure the validity of the current conservation condition separately for every term or corresponding diagram of Eq. (4) for the scattering amplitude. This property follows from the three-momentum conservation in the intermediate states for every term in the considered formulation. In the Coulomb gauge it is necessary to introduce transversal field operators that satisfy the modified commutation relations. Afterwards one can build the corresponding S-matrix reduction formulas given by Bjorken and Drell [11]. In particular, the photon current operator must be replaced by the following transversal operator:

$$J_\mu(x) \Longrightarrow J^{tr}_{\mu=i=1,2,3}(x) = J_i(x) - \frac{\nabla_i \partial_o}{\nabla^2} J_o(x). \qquad (7)$$

The time component $\mu = o$ of the transverse current operator $J^{tr}_\mu(x)$ [Eq. (7)] is excluded from the exact consideration. The replacement [Eq. (7)] generates the following redefinition

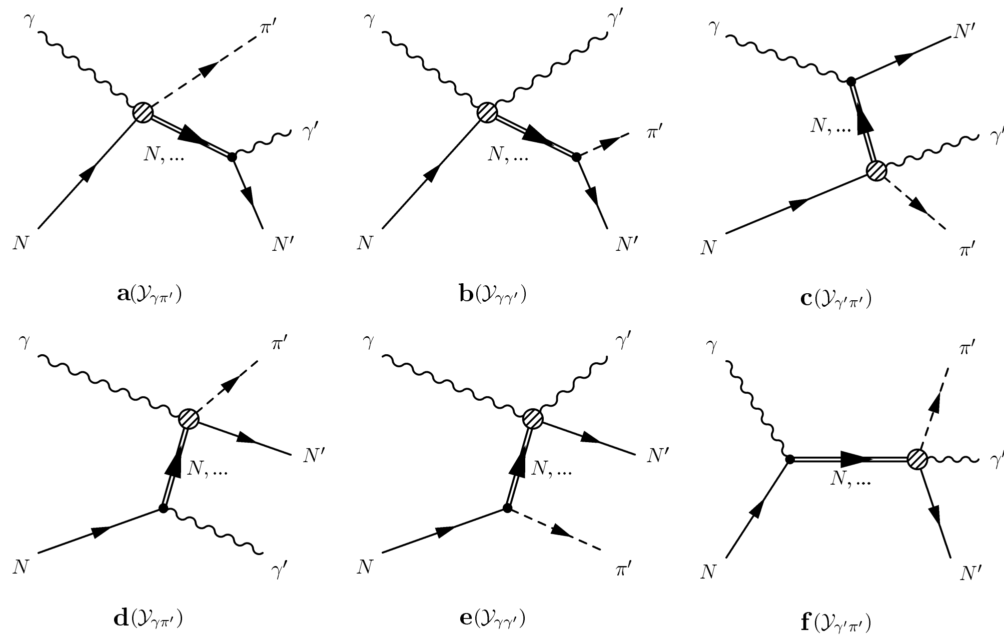

FIG. 3. Diagrammatic representation of the second part of Eq. (2) with the equal-time commutators for the photon and pion operators (**a**, **c**, **d**, and **f**) and the γ, γ' operators (**b** and **e**). **3a** corresponds to the expression in the curly brackets of Eq. (3b).

of the nucleon electromagnetic vertex function

$$\begin{aligned}\langle \mathbf{p}'_N|J_i^{tr}(0)|\mathbf{p}_N\rangle &= \langle \mathbf{p}'_N|J_i(0)|\mathbf{p}_N\rangle \\ &\quad - \frac{(\mathbf{p}'_\mathbf{N}-\mathbf{p}_\mathbf{N})_i(E_{\mathbf{p}'_N}-E_{\mathbf{p}_N})}{(\mathbf{p}'_\mathbf{N}-\mathbf{p}_\mathbf{N})^2} \\ &\quad \times \langle \mathbf{p}'_N|J_o(0)|\mathbf{p}_N\rangle. \end{aligned} \tag{8}$$

The current conservation condition $\partial^\mu J_\mu(x)=0$ implies the condition for the modified current $\partial^i J_i^{tr}(x)=0$. In the considered formulation the complete three-momentum of an arbitrary transition matrix element between the n and $\gamma+m$ particle states $\langle n|J_i(0)|m\rangle$ is conserved $\mathbf{k}_\gamma=\mathbf{P_n}-\mathbf{P_m}$. Therefore the relations $\partial^\mu J_\mu(x)=0$ and $\partial^i J_i^{tr}(x)=0$ generate the current conservation condition in the matrix form:

$$\mathbf{k}_\gamma^i\langle n|J_i^{tr}(0)|m\rangle=0. \tag{9a}$$

This condition simplifies the proof of the current conservation in Eqs. (2) and (4). In particular, using Eq. (9a) we get the following:

$$\begin{aligned}\mathbf{k}_\gamma^j\mathcal{T}_{ij} &= \mathbf{k}_\gamma^j\langle \text{out}; \mathbf{p}'_N\mathbf{p}'_\pi\mathbf{k}'_\gamma i|J_j^{tr}(0)|\mathbf{p}_N\rangle=0 \\ &= (2\pi)^6\sum_{\text{permutation}\,\gamma\gamma'\pi'}\Bigg\{\sum_{n,m}\langle \mathbf{p}'_N|J_i^{tr}(0)|m;in\rangle \\ &\quad\times\frac{\delta(\mathbf{k}'_\gamma+\mathbf{p}'_\mathbf{N}-\mathbf{P_m})}{E_{k'_\gamma}+E_{p'_N}-P_m^o+io}\langle in;m|j_{\pi'}(0)|n;in\rangle \\ &\quad\times\frac{\delta(\mathbf{k}'_\gamma+\mathbf{p}'_\mathbf{N}+\mathbf{p}'_\pi-\mathbf{P_n})}{E_{k'_\gamma}+E_{p'_N}+E_{p'_\pi}-P_n^o+io}\mathbf{k}_\gamma^j\langle in;n|J_j^{tr}(0)|\mathbf{p}_N\rangle\Bigg\} \\ &\quad+\mathbf{k}_\gamma^j\{\text{equal time commutators}\}_{ij}=0, \end{aligned} \tag{9b}$$

because $\mathbf{k}'_\gamma+\mathbf{p}'_N+\mathbf{p}'_\pi=\mathbf{P}_n=\mathbf{k}_\gamma+\mathbf{p}_N$. Taking into account that

$$\begin{aligned}\mathbf{k}_\gamma^j\mathcal{Y}_{ij} &= \sum_{\text{permutation}\,\gamma\,\gamma'\,\pi'}\int d^4x\int dy_o e^{ik'_\gamma x}\langle \mathbf{p}'_N| \\ &\quad\times J_i^{tr}(x)\theta(x_o-y_o)\delta(y_o)\big[a_{p_{\pi'}}(y_o), i\partial^j J_j^{tr}(0)\big]|\mathbf{p}_N\rangle \end{aligned} \tag{10a}$$

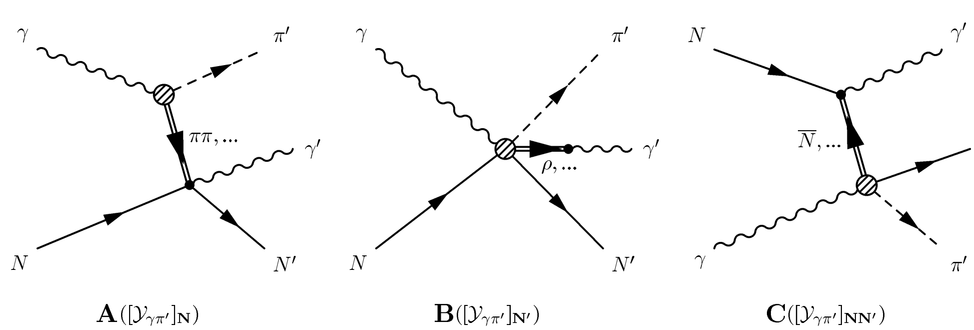

FIG. 4. New types of skeleton diagrams that appear after the cluster decomposition in Eq. (3b).

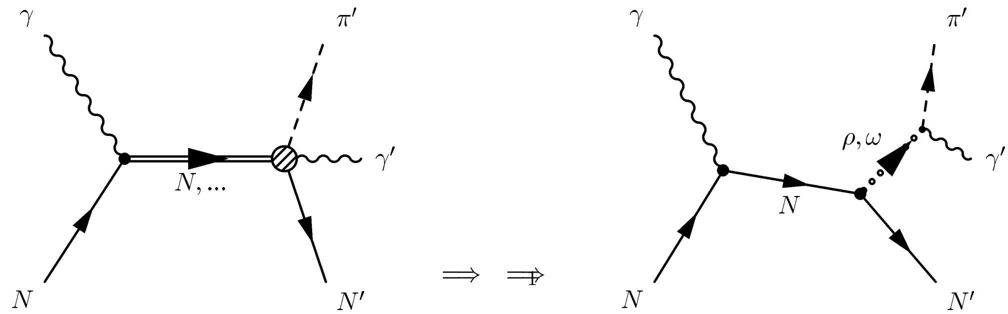

FIG. 5. One off-mass shell ρ-, ω-meson exchange diagram that is generated by the equal-time commutator [Eq. (6)] and calculated using the Lagrangian [Eq. (5)].

we see that

$$\mathbf{k}_{\gamma}^{j}\{\text{equal time commutators}\}_{ij} = 0. \tag{10b}$$

Thus the current conservation conditions (10b), (10c) are automatically satisfied if $J_{\mu}(0)$ and $J_{\nu}(0)$ are replaced by $J_i^{tr}(0)$ and $J_j^{tr}(0)$.

$$\mathbf{k}'^{i}_{\gamma}\mathcal{T}_{ij} = 0; \quad \mathbf{k}'^{i}_{\gamma}\{\text{equal time commutators}\}_{ij} = 0. \tag{10c}$$

For the simplest Lagrangian (2.9), the corresponding current operators and equal-time commutators satisfy the conditions [Eqs. (10b) and (10c)] if $J_{\mu}(0)$ and $J_{\nu}(0)$ are replaced by $J_i^{tr}(0)$ and $J_j^{tr}(0)$.

This completes the proof of the gauge invariance in the considered formulation. Other details of the current conservation condition in the same formulation are given in Ref. [10].

We note that in this three-dimensional time-ordered formulation for every diagram from the corresponding perturbation series the current conservation condition is fulfilled. Therefore here it is not necessary to use some additional approximations such as the tree approximation with a gauge invariant combination of terms [25], the construction of approximate auxiliary gauge-invariance-preserving currents [29,27,30], or to use the special representation of the off-mass shell Δ propagator and the corresponding construction of the gauge invariant electromagnetic Δ vertex function [7,18,4] to achieve the gauge invariance (current conservation) condition. Moreover, we have not to apply the four-dimensional Ward-Takahashi identities to get the current conservation condition and the problems concerning with the robustness of the seagull (overlapping or contact) terms [28] does not arise in the considered three-dimensional formulation.

Finally, we note that the Coulomb gauge simplifies the practical calculations in the three-dimensional time-ordered field-theoretical formulations (see, for example, the last paragraph of chapter 3 in Ref. [17]). Comparing this gauge with the Lorentz gauge in the four-dimensional exact covariant formulations, we see that for the Coulomb gauge it is not necessary to redefine the scalar product (i.e., to introduce an indefinite metric). These redefinitions are important for the calculations in Lorentz gauge for the four-dimensional Bethe-Salpeter-type equations in higher order than the tree approximation. Besides, in the Lorentz gauge the current conservation condition is often determined only for the special combinations of the diagrams in the tree approximation.

IV. ON-MASS SHELL Δ EXTRACTION FROM THE INTERMEDIATE πN INTERACTIONS

The extraction of the Δ resonance from the intermediate πN states may be carried out by replacement of the Green function of the interacting πN system

$$\mathcal{G}^{\pi N}(E, \mathbf{p}_{\Delta}) = \int d^3\mathbf{p} \frac{|\Psi_{\mathbf{p}}^{\pi N}\rangle\langle\widetilde{\Psi}_{\mathbf{p}}^{\pi N}|}{E - E_{\pi N}(\mathbf{p}, \mathbf{p}_{\Delta}) + io}, \tag{11}$$

with the equivalent formula with the intermediate Δ resonance state

$$\mathcal{G}^{\pi N}(E, \mathbf{p}_{\Delta}) = \sum_{\Delta} \frac{|\Psi_{\mathbf{p}_{\Delta}}\rangle\langle\widehat{\Psi}_{\mathbf{p}_{\Delta}}|}{E - E_{\mathbf{p}_{\Delta}} - \Sigma_{\Delta}(E, \mathbf{p}_{\Delta})} + \text{nonresonant part}, \tag{12}$$

where $E_{\mathbf{p}_{\Delta}} = \sqrt{\mathbf{p}_{\Delta}^2 + m_{\Delta}^2}$ and m_{Δ} denote the energy and the mass of the intermediate Δ resonance. The Δ mass operator $\Sigma_{\Delta}(E, \mathbf{p}_{\Delta})$ has a different form in different models of the off-mass shell Δ propagators. The symbols $\widetilde{\Psi}$ and $\widehat{\Psi}$ stands for the properly normalized wave functions of the πN and Δ states. This normalization is generated by the energy dependence of the effective πN potential $U(E) = A + EB$ [20,23,2].

The replacement of the complete Green function [Eq. (11)] by the spectral decomposition formula [Eq. (12)] with the intermediate Δ-resonance state can be considered a definition of the propagator of the intermediate off shell Δ. The Δ-propagator [Eq. (12)] is given off mass shell because the mass operator $\Sigma_{\Delta}(E, \mathbf{p}_{\Delta})$ is depending on the off shell energy parameter E. The accuracy of the replacement $\mathcal{G}^{\pi N}(E, \mathbf{p}_{\Delta})$ in Eq. (11) by $\mathcal{G}^{\pi N}(E, \mathbf{p}_{\Delta})$ in Eq. (12) determines the accuracy of the model for the off-energy shell Δ propagator [Eq. (12)]. In the center-of-mass (c.m.) frame $\mathbf{p}_{\Delta} = 0$ and in the Δ resonance region the mass operator $\Sigma_{\Delta}(E, \mathbf{p}_{\Delta})$ generates the Δ decay width at $E = m_{\Delta} = 1232$ MeV for the on shell πN amplitude. In this region the on-shell amplitude for the πN P_{33} partial wave has the Breit-Wigner form. This property can be used as the general normalization conditions for the Δ propagator [32]:

$$\mathrm{Re}[E - E_{\mathbf{p}_{\Delta}} - \Sigma_{\pi N}(E, \mathbf{p}_{\Delta})]_{E=m_{\Delta}}^{\mathbf{p}_{\Delta}=0} = 0 \tag{13a}$$

$$\mathrm{Im}[E - E_{\mathbf{p}_{\Delta}} - \Sigma_{\pi N}(E, \mathbf{p}_{\Delta})]_{E=m_{\Delta}}^{\mathbf{p}_{\Delta}=0} = \Gamma_{\Delta}/2. \tag{13b}$$

According to the modern πN phase shift analysis [34] the Breit-Wigner mass and width $m_{\Delta} = 1232$ MeV, $\Gamma_{\Delta} = 120$ MeV, differ from the Δ-pole mass and width

$m_\Delta^{\rm pole} = 1210$ MeV, $\Gamma_\Delta{}^{\rm pole} = 100$ MeV. In Sec. VI we demonstrate the sensitivity of our calculations to the above difference of the Δ mass and width for the $\gamma p - \pi^o p$ and $\gamma p - \gamma p$ reactions.

In the quantum field theory any transition between the $n + a$ and $m + b$ particle states ($n + a \Longleftarrow m + b$) with intermediate πN state is described by the following formula:

$$\sum_{\pi N} \langle n|j_a(0)|\mathbf{p}_\pi \mathbf{p}_N\rangle \frac{\delta(\mathbf{p}_a + \mathbf{P}_n - \mathbf{p}_\pi - \mathbf{p}_N)}{P_n{}^o + E_{\mathbf{p}_a} - E_{\mathbf{p}_\pi} - E_{\mathbf{p}_N} + io} \times \langle \mathbf{p}_\pi \mathbf{p}_N|j_b(0)|m\rangle = \sum_{\pi N} \langle n|j_a(0)||\mathbf{p}_\pi \mathbf{p}_N\rangle_{\pi N\,\text{irreducible}} \times \mathcal{G}^{\pi N}\big(E = P_n{}^o + E_{\mathbf{p}_a}\big)\langle \mathbf{p}_\pi \mathbf{p}_N|j_b(0)|m\rangle_{\pi N\,\text{irreducible}}, \tag{14}$$

which after replacement of Eq. (11) with Eq. (12), can be rewritten as follow:

$$\sum_{\pi N} \langle n|j_a(0)|\mathbf{p}_\pi \mathbf{p}_N\rangle \frac{\delta(\mathbf{p}_a + \mathbf{P}_n - \mathbf{p}_\pi - \mathbf{p}_N)}{P_n{}^o + E_{\mathbf{p}_a} - E_{\mathbf{p}_\pi} - E_{\mathbf{p}_N} + io} \times \langle \mathbf{p}_\pi \mathbf{p}_N|j_b(0)|m\rangle \simeq \sum_{\Delta} \{\langle n|j_a(0)\}_{\pi N\,\text{irreducible}}|\Psi_{\mathbf{p}_\Delta}\rangle \times \frac{\delta(\mathbf{p}_a + \mathbf{P}_n - \mathbf{p}_\Delta)}{P_n^o + E_{\mathbf{p}_a} - E_{\mathbf{p}_\Delta} - \Sigma_\Delta(E, \mathbf{p}_\Delta)} < \hat{\Psi}_{\mathbf{p}_\Delta}\{|j_b(0)|m\rangle\}_{\pi N\,\text{irreducible}}, \tag{15}$$

where we have neglected the nonresonant part of P_{33} πN partial-wave contributions.

In Eq. (15) is given the recipe of substitution the intermediate πN P_{33} partial-wave state for the intermediate Δ state. Unlike other formulations, we have not used an effective spin 3/2 Lagrangian to introduce the intermediate Δ's. Any spin 3/2 Lagrangian has free parameters corresponding to the off-mass shell degrees of freedom for the massive spin 3/2 particles. Therefore in the approach based on the effective spin 3/2 Lagrangian's, additional conditions are necessary to determine the actual off-mass shell behavior of the amplitude.

V. SEPARABLE MODEL OF THE π N AMPLITUDE AND PROPAGATOR OF THE INTERMEDIATE Δ RESONANCE

Equation (12) allows us to represent the propagator of the intermediate Δ in the following form

$$S_\Delta^{\alpha\beta}(E, \mathbf{p}_\Delta) = \frac{u^\alpha(\mathbf{p}_\Delta)\overline{u}^\beta(\mathbf{p}_\Delta)}{E - E_{\mathbf{p}_\Delta} - \Sigma_{\pi N}(E, \mathbf{p}_\Delta)} \frac{m_\Delta}{E_{\mathbf{p}_\Delta}}, \tag{16}$$

where $u^\alpha(\mathbf{p}_\Delta)$ is the spinor of the spin 3/2 particle with the real mass $m_\Delta = 1232$ MeV. In Eq. (16) and everywhere below we use the normalization condition for fermions from Ref. [12].

In this section our purpose is to determine the πN scattering amplitude through the propagator [Eq. (16)] in the framework of the separable model of the πN amplitude for the P_{33} partial wave. In the c.m. frame the πN amplitude with the intermediate Δ-isobar propagator has a separable form

$$\mathcal{A}_{\pi' N' - \Delta - \pi N}(\mathbf{p}'s', \mathbf{p}s; E) = g_{\pi' N' - \Delta}(\mathbf{p}') \frac{\mathcal{D}_\Delta(\mathbf{p}'s', \mathbf{p}s)}{E - m_\Delta - \Sigma_{\pi N}(E)} g_{\Delta - \pi N}(\mathbf{p}), \tag{17a}$$

where $\mathbf{p}', s'$ and $\mathbf{p}, s$ stands for the nucleon momenta and the spin in the final and in the initial states. In the c.m. frame $\mathbf{p}_\Delta = 0$, $p_\Delta^\mu = m_\Delta \delta^{\mu 0}$, $\mathbf{p}'^2_N = \mathbf{p}^2_N \equiv \mathbf{p}^2$, $E_{\mathbf{p}'} = E_{\mathbf{p}} = \sqrt{\mathbf{p}^2 + m_N^2}$ and

$$\mathcal{D}_\Delta(\mathbf{p}'s', \mathbf{p}s) = \overline{u}(\mathbf{p}')(p_\Delta - p'_N)_\alpha u^\alpha(0)\overline{u}^\beta(0)(p_\Delta - p_N)_\beta u(\mathbf{p}). \tag{17b}$$

Conversely, the πN scattering amplitude in the usual separable model for the resonance P_{33} partial waves has a form

$$T(\mathbf{p}'s', \mathbf{p}s; E) = v(\mathbf{p}') \frac{\mathcal{P}_1^{3/2}(\mathbf{p}'s', \mathbf{p}s)}{\lambda^{-1} - K_\Delta(E)} v(\mathbf{p}), \tag{18a}$$

where

$$K_\Delta(E) = \int \frac{d^3\mathbf{q}}{(2\pi)^3} \frac{m_N}{2E_{\mathbf{q}_\pi} E_{\mathbf{q}_N}} \frac{v^2(\mathbf{q})}{E + io - E_{\mathbf{q}_\pi} - E_{\mathbf{q}_N}} \tag{18b}$$

and $\mathcal{P}_1^{3/2}$ is the well known quantum-mechanical projection operator on the πN state with the angular momenta $L = 1$ and the total momenta $J = 3/2$ [11,13]

$$\mathcal{P}_1^{3/2}(\mathbf{p}'s', \mathbf{p}s) = \frac{3(\mathbf{p}'\mathbf{p})}{4\pi \mathbf{p}^2} \chi_f^+ \chi_i - \frac{1}{4\pi \mathbf{p}^2} \chi_f^+ (\mathbf{p}'\sigma)(\sigma \mathbf{p})\chi_i = \frac{3m_N(\mathbf{p}'\mathbf{p})}{4\pi \mathbf{p}^2(E_{\mathbf{p}} + m_N)} \overline{u}(\mathbf{p}'s')(1 + \gamma_o)u(\mathbf{p}s) - \mathcal{P}_1^{1/2}(\mathbf{p}'s', \mathbf{p}s), \tag{19a}$$

where $u(\mathbf{p}s)$ is the spinor function of nucleon, $u(0s') = \chi_f$, $u(0s) = \chi_i$, and

$$\mathcal{P}_1^{1/2}(\mathbf{p}'s', \mathbf{p}s) = \frac{1}{4\pi \mathbf{p}^2} \chi_f^+ (\mathbf{p}'\sigma)(\sigma \mathbf{p})\chi_i = \frac{m_N(E_{\mathbf{p}} + m_N)}{4\pi \mathbf{p}^2} \overline{u}(\mathbf{p}'s')(\gamma_o - 1)u(\mathbf{p}s) \tag{19b}$$

$$\mathcal{P}_0^{1/2}(\mathbf{p}'s', \mathbf{p}s) = \frac{1}{4\pi} \chi_f^+ \chi_i = \frac{m_N}{4\pi(E_{\mathbf{p}} + m_N)} \overline{u}(\mathbf{p}'s')(\gamma_o + 1)u(\mathbf{p}s). \tag{19c}$$

These projectors satisfy the idempotency condition

$$\sum_{s''} \int d\Omega_{\mathbf{p}''} \big[\mathcal{P}_{L'}^{J'}(\mathbf{p}''s'', \mathbf{p}'s')\big]^+ \mathcal{P}_L^J(\mathbf{p}''s'', \mathbf{p}s) = \delta_{L'L}\delta_{J'J}\mathcal{P}_L^J(\mathbf{p}'s', \mathbf{p}s). \tag{19d}$$

Using the identity $(p^\sigma\gamma_\sigma + m)\gamma_0(p^\delta\gamma_\delta + m) = 2E_{\mathbf{p}}(p^\sigma\gamma_\sigma + m)$ it is easy to derive the following relation:

$$\mathcal{D}_\Delta(\mathbf{p}'s', \mathbf{p}s) = \frac{4\pi \mathbf{p}^2(E_{\mathbf{p}} + m_N)}{6m_N} \mathcal{P}_1^{3/2}(\mathbf{p}'s', \mathbf{p}s), \tag{20}$$

where we have used the following representation for the spin 3/2 particle projection operator [14–16,19]

$$u^{\mu}(\mathbf{p}_{\Delta})\overline{u}^{\nu}(\mathbf{p}_{\Delta}) = -\frac{p^{\sigma}_{\Delta}\gamma_{\sigma}+m_{\Delta}}{2m_{\Delta}}\left[g^{\mu\nu}-\frac{1}{3}\gamma^{\mu}\gamma^{\nu}-\frac{1}{3m_{\Delta}^{2}}\right.$$
$$\left.\times\left(\gamma_{\sigma}p^{\sigma}_{\Delta}\gamma^{\mu}p^{\nu}_{\Delta}+\gamma^{\mu}p^{\nu}_{\Delta}\gamma_{\sigma}p^{\sigma}_{\Delta}\right)\right], \qquad (21a)$$

which involves only the contributions of the $L = 1$ and $J = 3/2$ partial state.

Equation (21a) differs from the other representation of the spin 3/2 particle projection operator that is often found in the literature [17,18,4]

$$u^{\mu}(\mathbf{p}_{\Delta})\overline{u}^{\nu}(\mathbf{p}_{\Delta}) = -\frac{p^{\sigma}_{\Delta}\gamma_{\sigma}+m_{\Delta}}{2m_{\Delta}}\left[g^{\mu\nu}-\frac{1}{3}\gamma^{\mu}\gamma^{\nu}\right.$$
$$\left.-\frac{2}{3m_{\Delta}^{2}}p^{\mu}_{\Delta}p^{\nu}_{\Delta}-\frac{1}{3m_{\Delta}}\left(\gamma^{\mu}p^{\nu}_{\Delta}-\gamma^{\mu}p^{\nu}_{\Delta}\right)\right], \qquad (21b)$$

which can be decomposed over the other kind of the projection operators [14,16]

$$[P^{3/2}]^{\mu\nu} = g^{\mu\nu}-\frac{1}{3}\gamma^{\mu}\gamma^{\nu} - \frac{1}{3m_{\Delta}^{2}}\left(\gamma_{\sigma}p^{\sigma}_{\Delta}\gamma^{\mu}p^{\nu}_{\Delta}+\gamma^{\mu}p^{\nu}_{\Delta}\gamma_{\sigma}p^{\sigma}_{\Delta}\right) \qquad (22a)$$

$$\left[P^{1/2}_{11}\right]^{\mu\nu} = \frac{1}{3}\gamma^{\mu}\gamma^{\nu}-\frac{1}{m_{\Delta}^{2}}p^{\mu}_{\Delta}p^{\nu}_{\Delta} + \frac{1}{3m_{\Delta}^{2}}\left(\gamma_{\sigma}p^{\sigma}_{\Delta}\gamma^{\mu}p^{\nu}_{\Delta}+\gamma^{\mu}p^{\nu}_{\Delta}\gamma_{\sigma}p^{\sigma}_{\Delta}\right). \qquad (22b)$$

$$\left[P^{1/2}_{22}\right]^{\mu\nu} = \frac{1}{m_{\Delta}^{2}}p^{\mu}_{\Delta}p^{\nu}_{\Delta} \qquad (22c)$$

$$\left[P^{1/2}_{12}\right]^{\mu\nu} = \frac{1}{\sqrt{3}m_{\Delta}^{2}}\left(p^{\mu}_{\Delta}p^{\nu}_{\Delta}-\gamma_{\sigma}p^{\sigma}_{\Delta}\gamma^{\mu}p^{\nu}_{\Delta}\right) \qquad (22d)$$

$$\left[P^{1/2}_{21}\right]^{\mu\nu} = \frac{1}{\sqrt{3}m_{\Delta}^{2}}\left(\gamma_{\sigma}p^{\sigma}_{\Delta}\gamma^{\nu}p^{\mu}_{\Delta}-p^{\mu}_{\Delta}p^{\nu}_{\Delta}\right). \qquad (22e)$$

These projection operators satisfy a useful relations

$$[P^{3/2}]^{\mu\nu}+\left[P^{1/2}_{11}\right]^{\mu\nu}+\left[P^{1/2}_{22}\right]^{\mu\nu} = g^{\mu\nu} \qquad (23a)$$

$$\left[P^{J'}_{ij}\right]^{\mu\sigma}g_{\sigma\delta}\left[P^{J}_{kl}\right]^{\delta\nu} = \delta^{J'J}\delta_{jk}\left[P^{J}_{il}\right]^{\mu\nu}, \qquad (23b)$$

$$[P^{3/2}]^{\mu\nu}p^{\sigma}_{\Delta}\gamma_{\sigma} = p^{\sigma}_{\Delta}\gamma_{\sigma}[P^{3/2}]^{\mu\nu}. \qquad (23c)$$

In analog with the Dirac propagator for the spin 1/2 particle

$$S_{1/2}(E,\mathbf{p}) = \frac{u(\mathbf{p}s)\overline{u}(\mathbf{p}s)}{E-E_{\mathbf{p}}-\Sigma(E,\mathbf{p})}\frac{m}{E_{\mathbf{p}}},$$

the spin 3/2 particle propagator [Eq. (16)] contains the projection operator $u^{\alpha}(\mathbf{p}_{\Delta})\overline{u}^{\beta}(\mathbf{p}_{\Delta})$ on the positive energy states. Therefore, the propagator [Eq. (16)] has no inverse operator. Nevertheless, one can consider

$$\left(P^{3/2}{}_{\mu\nu}p^{\sigma}_{\Delta}\gamma_{\sigma}-m_{\Delta}g_{\mu\nu}\right)\Psi^{\nu} = 0$$

as equation of motion of the spin 3/2 particle that is equivalent to the equation

$$\left(p^{\sigma}_{\Delta}\gamma_{\sigma}-m_{\Delta}\right)\Psi^{\nu} = 0.$$

To proof this statement, one can use the relations [Eqs. (23a)–(23b)] and the property of operators $\Psi^{\nu} = [P^{3/2}]^{\nu\mu}\Psi_{\mu}$ that is result of the definition of these operators in the subspace for the free spin 3/2 particles. This allows us to avoid the criticism given in Ref. [16] for the propagator

$$S^{\mu\nu}_{\Delta}(E,\mathbf{p}_{\Delta}) = -\frac{p^{\sigma}_{\Delta}\gamma_{\sigma}+m_{\Delta}}{2m_{\Delta}}\frac{[P^{3/2}]^{\mu\nu}}{E-E_{\mathbf{p}_{\Delta}}-\Sigma_{\pi N}(E,\mathbf{p}_{\Delta})}\frac{m_{\Delta}}{E_{\mathbf{p}_{\Delta}}}. \qquad (24)$$

Using the Eq. (20), one can express the propagator [Eqs. (16) and (24)] through the spin 3/2 projection operator [Eq. (19a)] and the Δ propagator

$$p'^{N}_{\mu}S^{\mu\nu}_{\Delta}(E)p^{N}_{\nu} = \frac{4\pi\mathbf{p}^{2}(E_{\mathbf{p}}+m_{N})}{6m_{N}}\frac{\mathcal{P}^{3/2}_{1}(\mathbf{p}'s',\mathbf{p}s)}{E-m_{\Delta}-\Sigma_{\pi N}(E)}, \qquad (25)$$

where $\Sigma_{\pi N}(E) = -E+m_{\Delta}+\lambda^{-1}-K_{\Delta}(E)$ for the separable models. Next if we define the relations between the form factors as follows:

$$v(\mathbf{p}')v(\mathbf{p}) = \frac{4\pi\mathbf{p}^{2}(E_{\mathbf{p}}+m_{N})}{6m_{N}}g_{\pi'N'-\Delta}(\mathbf{p}')g_{\Delta-\pi N}(\mathbf{p}), \qquad (26a)$$

then we obtain that the amplitude [Eq. (17a)] and the amplitude [Eq. (18a)] coincide

$$\mathcal{A}_{\pi'N'-\Delta-\pi N}(\mathbf{p}'s',\mathbf{p}s;E) = T(\mathbf{p}',\mathbf{p};E). \qquad (26b)$$

Equations (26a) and (26b) are our final result for the relation between the Δ separable amplitude [Eq. (18a)] with $L = 1; J = 3/2$ and the microscopic πN amplitude [Eq. (17a)] with the Δ propagator [Eq. (16)]. According to the well-known procedure in the separable model the form factors $v(\mathbf{p})$ as well as λ and $K_{\Delta}(E)$ can be determined through the πN phase shifts [9]. It is important to note that the amplitude in the separable model [Eq. (18a)] is scale invariant, because the variation of the λ scale parameter $\lambda' = \delta\lambda$ can be compensated by the corresponding variation of the form factors $v'(\mathbf{p}) = \delta^{-1/2}v(\mathbf{p})$.

To calculate the amplitude of the multichannel γp scattering reactions we have used the normalization condition of the Δ propagator [Eqs. (13a) and (13b)] because in the opposite case intermediate Δ propagators do not have the observed Δ decay width and the Δ pole position. Equations (13a) and (13b) violated the scale invariance of the separable πN t matrix. In our calculation we have used the following models of the πN propagator [Eqs. (16), (24), and (25)] and $\pi N-\Delta$ form factors $g(\mathbf{p})$ in the c.m. frame.

A. Scale-invariant separable model (Model A) [23]

In this model the πN scattering amplitude reproduce the the P_{33} partial wave πN phase shifts up to 300 MeV. The propagator of the Δ has the following form:

$$S^{\alpha\beta}_{\Delta}(E) = \frac{u^{\alpha}(0)\overline{u}^{\beta}(0)}{\lambda^{-1}-K_{\Delta}(E)}, \qquad (27)$$

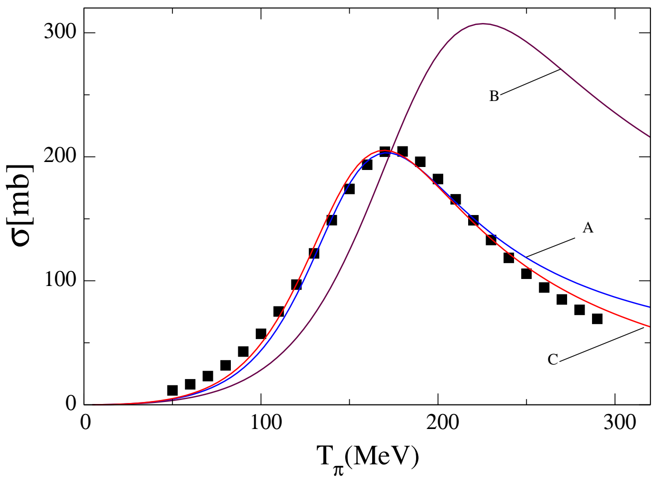

FIG. 6. (Color online) The integral cross sections of the $\pi^+ p$ scattering reaction calculated in the framework of the one Δ exchange model according to the Eqs. (35b) and (36b). Curve B is generated by the $\pi^+ p$ amplitude [Eq. (34)] with the Δ propagator in the relativistic Breit-Wigner shape model B [Eq. (29)]. Curves A and C are obtained using the unitary $\pi^+ p$ scattering amplitude [Eqs. (17a) and (18a)] and they coincide with the cross section constructed from the corresponding pion-nucleon phase shifts in the next figure. The data are taken from the SAID analysis [33].

where $K_\Delta(E)$ is defined in Eqs. (18a) and (18b) and

$$\lambda^{-1} = \mathrm{Re}[K_\Delta(E = m_\Delta)]; \quad g(\mathbf{p}) = \frac{\eta}{\mathbf{p}^2 + \mu^2} \tag{28}$$

with the following choice of the fitting parameters $\mu = 9m_\pi$, $\eta = 15.85m_N$.

The form of the λ^{-1} insures the validity of Eq. (13a) and the adjustable parameter η is fixed according to Eq. (13b).

B. Breit-Wigner shape Δ propagator (Model B) [2]

In this model $E_{\mathbf{p}_\Delta} + \Sigma_{\pi N}(E) \approx \sqrt{(m_\Delta - i\Gamma_\Delta/2)^2 + \mathbf{p}_\Delta^2}$ and the Δ propagator has the following form:

$$S_\Delta^{\alpha\beta}(E, \mathbf{p}_\Delta) = \frac{u^\alpha(\mathbf{p}_\Delta)\overline{u}^\beta(\mathbf{p}_\Delta)}{E - \sqrt{\left(m_\Delta - i\frac{\Gamma_\Delta}{2}\right)^2 + \mathbf{p}_\Delta^2}} \frac{m_\Delta}{E_{\mathbf{p}_\Delta}}. \tag{29}$$

The form factor $g(\mathbf{p})$ is obtained from the effective $\pi N\Delta$ Lagrangian in tree approximation (i.e., it is equal to the $g_{\pi N\Delta}$ coupling constant):

$$g(\mathbf{p}) = g_{\pi N\Delta}, \tag{30}$$

where we have taken the same coupling constant as in Ref. [4]$g_{\pi N\Delta} = 1.95/m_\pi$.

C. Heller-Kumano-Martinez-Moniz separable potential (model C) [32]

This model was used for the calculation of the Δ^{++} magnetic moment in the $\pi^+ p \to \gamma'\pi^+ p$ reaction and it reproduces the πN P_{33} phase shifts up to 300 MeV. In this model the following parametrization is used:

$$\begin{aligned} m_\Delta + \Sigma_{\pi N}(E) &\equiv M_\Delta + \tilde{\Sigma}_{\pi N}(E) \\ &= M_\Delta + \frac{1}{3}\int \frac{d^3\mathbf{q}}{(2\pi)^3} \frac{\mathbf{q}^2 h^2(\mathbf{q})}{E + io - E_{\mathbf{q}_\pi} - E_{\mathbf{q}_N}}, \end{aligned} \tag{31}$$

where $M_\Delta = 1322$ MeV is the "bare" Δ mass

$$h(\mathbf{q}) = \frac{g}{\left(1 + \frac{\mathbf{q}^2}{\alpha^2}\right)^2} \tag{32}$$

and $\alpha = 2.20\,\mathrm{fm}^{-1}$ and $g = 1.79\, m_\pi{}^{-3/2}$. Thus the Δ propagator in the Heller-Kumano-Martinez-Moniz separable potential model has the following form:

$$S_\Delta^{\alpha\beta}(E) = \frac{u^\alpha(0)\overline{u}^\beta(0)}{E - M_\Delta - \tilde{\Sigma}_{\pi N}(E)}. \tag{33}$$

Before we compare the cross sections of the $\gamma p \to \gamma' p'$, $\gamma p \to \pi^{o\prime} p'$, and $\gamma p \to \gamma'\pi^{o\prime} p'$ reactions in the Δ resonance region, calculated with the above Δ propagators, we have to examine the sensitivity of the πN scattering observables to the choice of the models of the Δ propagators. Unlike to the separable models of the πN amplitude with the Δ propagators A and C, the $\pi^+ p$ scattering amplitude constructed with the Breit-Wigner shape Δ propagator (5.12)

$$\begin{aligned} \mathcal{T}_{\pi^+ p}(\mathbf{p}', \mathbf{p}; E) &= g_{\pi N\Delta}^2 \frac{E_\mathbf{p} + m_N}{2m_N} \\ &\quad \times \frac{\left[\chi_f^+(\mathbf{p}'\mathbf{p})\chi_i - \frac{1}{3}\chi_f^+(\mathbf{p}'\sigma)(\sigma\mathbf{p})\chi_i\right]}{E - m_\Delta + i\frac{\Gamma_\Delta}{2}} \end{aligned} \tag{34}$$

does not satisfy the unitarity condition. Therefore this amplitude as well as a number of the other Breit-Wigner-type πN amplitudes often used for the description of the γN reactions (see, for example, Refs. [7,4]) are not able to reproduce πN scattering experimental observables without an additional unitarization procedure. In particular, for the $\pi^+ p$ scattering cross with the amplitude [Eq. (34)] the following explicit expression is valid [11]

$$\frac{d\sigma_{\pi^+ p}^B}{d\Omega} = g_{\pi N\Delta}^4 p^4 \frac{(E_\mathbf{p} + m_N)^2}{(24\pi E)^2} \frac{1 + 3\cos^2\theta}{(E - m_\Delta)^2 + \frac{\Gamma_\Delta^2}{4}}, \tag{35a}$$

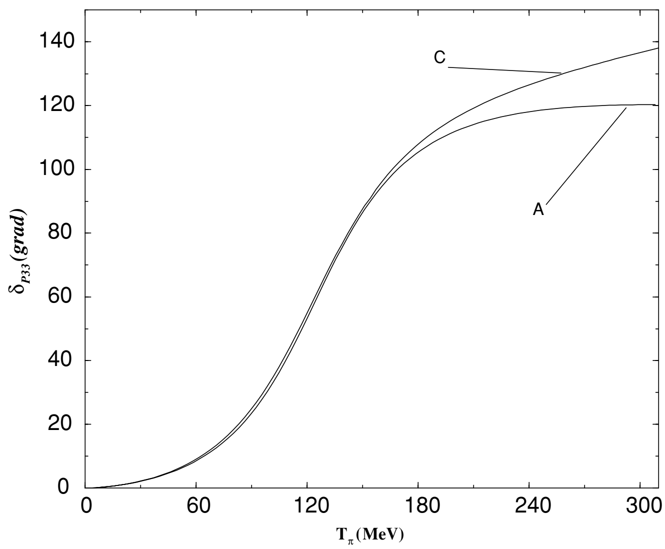

FIG. 7. $\pi N\, P_{33}$ phase shifts used in Ref. [23] (A) and in Ref. [32] (C). These curves describe well the πN phase from the corresponding phase-shift analyses.

$$\sigma^B_{\pi^+ p} = \frac{g^4_{\pi N\Delta} p^4}{2\pi} \frac{(E_{\mathbf{p}} + m_N)^2}{(6E)^2} \frac{1}{(E - m_\Delta)^2 + \frac{\Gamma^2_\Delta}{4}}. \qquad (35b)$$

This integral cross section, obtained in the framework of the Breit-Wigner shape model for the Δ propagator [Eq. (29)] is depicted in Fig. 6 together with the cross sections calculated with the $\pi^+ p$ separable amplitudes in model A [23] and model C [32]. For the cross sections, calculated in the framework of the separable models A and C are valid the analogical to the Eqs. (35a) and (35b) expressions

$$\frac{d\sigma^{A,C}_{\pi^+ p}}{d\Omega} = [g_{\pi N-\Delta}(\mathbf{p}^2)p]^4 \frac{(E_{\mathbf{p}} + m_N)^2}{(24\pi E)^2} \times \frac{1 + 3\cos^2\theta}{|E - m_\Delta - \Sigma_{\pi N}(E)|^2}, \qquad (36a)$$

$$\sigma^{A,C}_{\pi^+ p} = \frac{[g_{\pi N-\Delta}(\mathbf{p}^2)p]^4}{2\pi} \frac{(E_{\mathbf{p}} + m_N)^2}{(6E)^2} \times \frac{1}{|E - m_\Delta - \Sigma_{\pi N}(E)|^2}. \qquad (36b)$$

Unlike curves A and C, curve B presents the essentially non-realistic description of the $\pi^+ p$ integral cross section. In order to improve the relativistic Breit-Wigner shape model it was suggested the different unitarization procedures [20,22,23] these procedures use the special separation of the resonance and the non-resonance parts of the P_{33} πN partial phase shifts with the additional fit of the adjustable parameters. In the separable model of the πN amplitude (17a) or (18a) the unitarity condition is satisfied and the form factors as well as the $\Sigma_\Delta(E)$ or $K_\Delta(E)$ functions are explicitly determined via the observed πN P_{33} partial wave shifts (see for example [7] and the references therein).

It is seen that at the peak of the Δ resonance the difference between curves A and C is small. But after the $T_\pi > 200$ MeV the difference between curves A and C is essential. This difference is generated by the difference between the πN phase shift analyses (see the next figure), which was used in the construction of the $g(\mathbf{p})$ and $h(\mathbf{p})$ form factors curves A and C.

The resonance P_{33} πN phase shifts for curves A and C are presented in Fig. 7. These curves practically coincides with the corresponding data from the phase-shift analyzes performed in Ref. [45] (model A) and in ref. [32] (model C) correspondingly. The difference between the curves is visible after $T_\pi = 150$ MeV. This difference is more transparent for the πN total cross section depicted in Fig. 6. Because of the unitarity breaking for the πN amplitude [Eq. (34)] (B), it is not possible to extract the phase shifts from this expression. The generalized relativistic Breit-Wigner shape Δ propagator and the corresponding $\pi^+ p$ scattering amplitude, which satisfy the unitarity condition and which reproduce the correct P_{33} phase shifts and the πN cross section was constructed in Refs. [16,18,19].

VI. THE RESULTS FOR THE $\gamma p \to \gamma' p'$, $\gamma p \to \pi^{o\prime} p'$, AND $\gamma p \to \gamma' \pi^{o\prime} p'$ OBSERVABLES IN THE Δ RESONANCE REGION

In this section we examine the dependence of the observables of the $\gamma p \to \gamma' p'$, $\gamma p \to \pi^{o\prime} p'$, and $\gamma p \to \gamma' \pi^{o\prime} p'$ reactions on the above referred Δ propagators to study the sensitivity of the cross sections of the $\gamma p \to \gamma' \pi^{o\prime} p'$ reaction to the magnitude of the Δ^+ magnetic moment in different kinematical regions.

Our numerical calculation is restricted to the one-particle N, Δ, π, and ρ-, ω-exchange model that was applied in the most of the numerical calculations of these reactions. We will study the $\gamma p - \gamma p$, $\gamma p - \pi^o p$, and $\gamma p - \gamma \pi^o p$ reactions in the unified manner with the same input vertex functions to compare with the preliminary experimental data [5]. The already well-investigated proton Compton scattering reaction is the same order as the $\gamma p - \gamma \pi N$ reaction (in nb). Therefore inclusion of the $\gamma p - \gamma p$ reaction in our consideration is consistent. In the Δ resonance region the $\gamma p \to \gamma p$ reaction separately was well described in the tree approximation in Ref. [7]. In the same approximation the unified description of the $\gamma p \to \pi^o p$ and $\gamma p \to \gamma \pi^o p$ reactions was achieved in Ref. [4]. Our calculations are performed in the Born approximation that is more general as the tree approximation. In the Born approximation it is possible to examine the sensitivity of the calculated cross sections to the separable model of the Δ resonance. The separable model insures the validity of the unitarity condition for the Δ-exchange $\pi N - \pi N$ amplitude, but in the considered Born approximation of the $\gamma N - \gamma \pi N$ amplitude the unitarity condition is violated. Nevertheless this approximation is more complete as the tree approximation, where the unitarity condition is broken by description of the $\pi N - \pi N$, $\gamma p - \pi p$, $\gamma p - \gamma p$, and $\gamma p - \gamma \pi p$ reactions. Generalization of the three-dimensional time-ordered equations for the πN scattering amplitude [20,23] is given in Ref. [10] for the coupled $\pi N - \gamma N - \pi\pi N - \gamma \pi N$

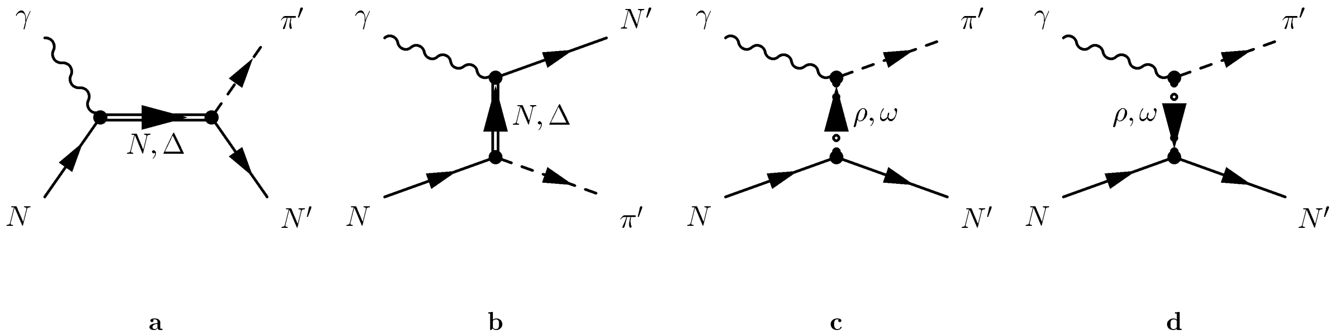

FIG. 8. Diagrams for the π^o photoproduction on the proton. One-particle N, Δ and ρ-, ω-exchange diagrams taken into account in the numerical calculation of the $\gamma p - \pi^{o\prime} p'$ reaction.

channels, where the two-body and the three-body unitarity conditions are satisfied. Therefore the present investigation can be considered as a preliminary step for the unified and the quantitative description of the multichannel γp and πN scattering reactions. On this stage of our calculations we have not taken into account the contributions of the nonresonant πN partial waves and the antinucleon degrees of freedom in the intermediate states of the πN interaction (i.e., in the present article we are able to consider only a qualitative effects in the multichannel γp reactions).

A. Pion photoproduction reaction

Our calculation of the $\gamma p \to \pi^{o\prime} p'$ reaction based on the same set of diagrams as in Ref. [25], but our calculation is performed in the three-dimensional, time-ordered form in the Coulomb gauge and without neglection of the off-mass shell variables in the vertex functions. Therefore we have two-type ρ-, ω-exchange diagrams with the linear propagators that differ in the chronological sequences of the intermediate ρ, ω emission and absorption as it is shown in diagrams **c** and **d** in Fig. 8. The corresponding vector-meson $V \equiv \rho, \omega$ exchange diagrams have the different propagators $(E_{\mathbf{p}_N} - E_{\mathbf{p}'_N} + E_{\mathbf{p}_V})^{-1}$ and $(E_{\mathbf{p}_N} - E_{\mathbf{p}'_N} - E_{\mathbf{p}_V})^{-1}$. These t and $\bar{t}$ channel terms with the ρ-, ω-meson exchange (diagrams **c** and **d**) are important for our calculation. The N, Δ exchange diagrams (**a** and **b**) relate to the s-, and u-channel interaction terms. The $\bar{s}$-, and $\bar{u}$-channel terms with $\overline{N}, \overline{\Delta}$ exchange include the propagators $(E_{\mathbf{p}_N} + E_{\mathbf{p}'_N} \pm E_{\mathbf{p}_\pi})^{-1}$ and $(E_{\mathbf{p}_N} + E_{\mathbf{p}'_\Delta} \pm E_{\mathbf{p}_\pi})^{-1}$. These propagators are small in the Δ resonance region and they can be safely neglected.

The s- and u-channel diagrams (**a** and **b**) together with the $t, \bar{t}$-channel diagrams (**c** and **d**) are used for the calculation of the amplitude of the $\gamma p \to \pi^o p$ reaction in the Born approximation. The corresponding vertex function are listed in the appendix. With respect to the Δ-resonance propagator, the calculation was performed as follows: (curve A) for the scale-invariant separable model of the P_{33} πN amplitude [Eq. (27)] [23], (curve B) with the Breit-Wigner form of the Δ-resonance propagator [Eq. (29)], and (curve C) with the the separable model of the πN potential [32]. The resulting integral cross sections are presented in Fig. 9, where the curves A, B and C denote the calculations of all of the diagrams in Fig. 8 with the corresponding models A, B, and C of the Δ propagators.

As shown in Fig. 9, the peaks of curves A and C are removed from the position of the peak of the $\pi^+ p - \pi^+ p$ reaction at $T_\pi = 154$ MeV (or $E_\gamma = 340$ MeV or $E = m_\Delta = 1232$ MeV) into the position of the experimentally observed peak of the $\gamma p - \pi^o p$ integral cross section at $E_\gamma = 320$ MeV (or $T_\pi = 140$ MeV or $E = \overline{m}_\Delta = 1218$ MeV). The Δ propagators of the considered curves A, B, and C satisfy Eqs. (13a) and (13b) (i.e., they have the same Δ pole position at $E = m_\Delta = 1232$ MeV and the Δ decay width $\Gamma_\Delta = 120$ MeV). The curves $A_{\rm sh}$ and $C_{\rm sh}$ are obtained in the framework of the above separable Δ propagator models A and C, but with the removed Δ pole position at $E = \overline{m}_\Delta = 1210$ MeV and the Δ decay width $\overline{\Gamma}_\Delta = 100$ MeV. In Fig. 9 it is shown, that the peak of the $A_{\rm sh}$ and $C_{\rm sh}$ is again removed left at $E_\gamma = 285$ MeV. Thus despite

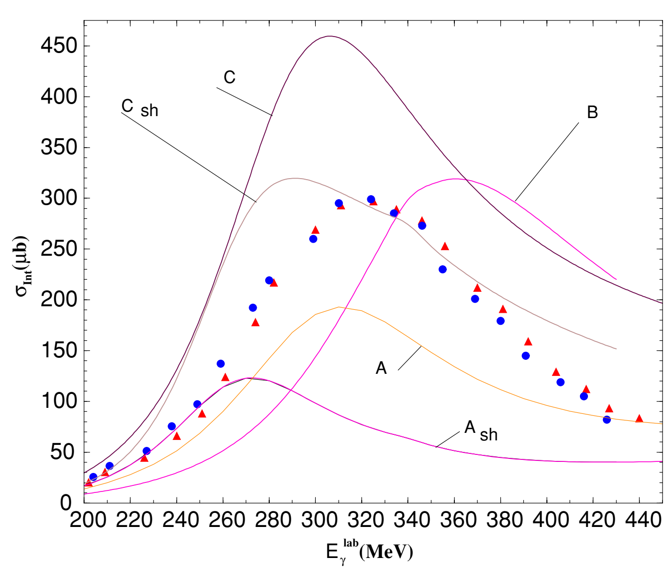

FIG. 9. (Color online) The integral cross sections of the pion photo-production reaction with models A [Eq. (27)], B [Eq. (29)], and C [Eq. (33)] of the Δ propagator. Curves A, B, and C are calculated with the Δ pole position at $E = m_\Delta = 1232$ MeV and with the Δ decay width $\Gamma_\Delta = 120$ MeV. Calculations for curves $A_{\rm sh}$ and $C_{\rm sh}$ are performed with $E = m_\Delta = 1210$ MeV and $\Gamma_\Delta = 100$ MeV. The experimental points are taken from Ref. [4].

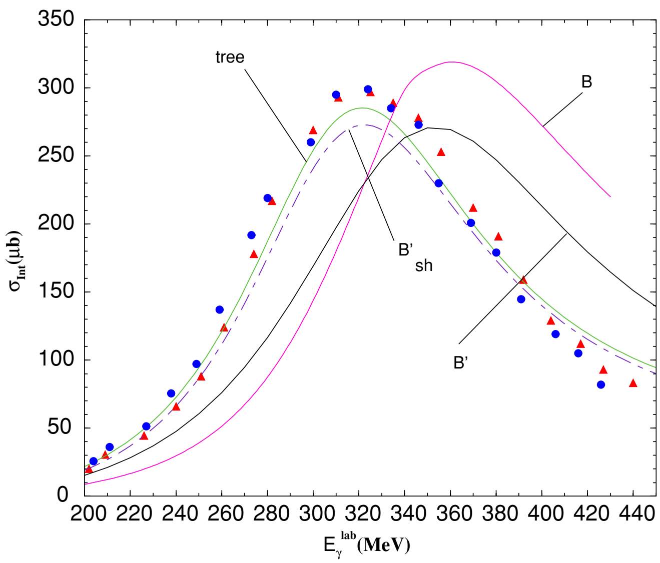

FIG. 10. (Color online) Comparison of our calculation of the $\gamma p \to \pi^o p$ integral cross section in model B with the analogical calculation in the three approximation [4]. The experimental points and curve B are the same as in the previous figure. Curve B' denotes the same calculation as for the case $B_{\rm born}$, but without Δ-exchange crossing term and without ρ-meson exchange term. Curve $B'_{\rm sh}$ is obtained in the same approximation as B' but with the shifted Δ pole parameters $m_\Delta = 1210$ MeV and $\Gamma_\Delta = 100$ MeV. The curve labeled *tree* stands for the calculation in the *tree* approximation as it was performed in Ref. [4]. This curve is obtained from $B'_{\rm sh}$ after tree approximation for all form factors and with the special model for the Δ propagator and the current conservation for the Δ-exchange term [18].

the same Δ pole position at $E = m_\Delta = 1232$ MeV and the Δ decay width $\Gamma_\Delta = 120$ MeV for the Δ propagator models A, B, and C, the corresponding peaks of the $\gamma p - \pi^o p$ integral cross section are removed. The displacement of the Δ pole position can be explained by the kinematical factors that appear together with the Δ propagator in the corresponding amplitude with the different form of the considered Δ propagators. Other example of the such type Δ pole position replacement is given in Fig. 6 for curve B, which is calculated according to Eq. (35b).

The magnitude of the calculated $\gamma p - \pi^o p$ integral cross section in curves A and C in Fig. 9 is sufficiently worse as curve B. Conversely, if we taken into account only the leading s-channel Δ exchange from diagram **a** in Fig. 8 then $\gamma p - \pi^o p$ scattering amplitude takes the separable form

$$\mathcal{T}^\mu_{\gamma p - \pi^o p}(\mathbf{p}', \mathbf{p}; E) \simeq \overline{u}(\mathbf{p}') F_M(t) \Gamma_M^{\mu\alpha}(t) \times \frac{u_\alpha(0)\overline{u}_\beta(0)}{\lambda^{-1} - K_\Delta(E)} p_N^\beta g_{\Delta-\pi N}(\mathbf{p}) u(\mathbf{p}), \tag{37}$$

where $F_M(t)$ and $\Gamma_M^{\mu\nu}(t)$ are given in Eq. (A2). Equation (37) satisfies the unitarity condition. Moreover, in the separable model $K_\Delta(E)$ function and the form factor $g_{\Delta-\pi N}(\mathbf{p}$ are determined via the πN P_{33} phase shifts in the πN energy region $m_N + m_\pi, \infty)$. Thus the $K_\Delta(E)$ function and the form factor $g_{\Delta-\pi N}(\mathbf{p}$ are essentially dependent on the asymptotic behavior of the πN scattering amplitude or on the πN phase shifts. We note that one can use the different separable models of the Δ propagators to estimate the accuracy of the performed calculations.

To compare our model with the calculations performed in the tree approximation, we make the same set of approximations as in Ref. [4] for reproduction of the $\gamma p \to \pi^{o\prime} p'$ integral cross section. The calculation in Ref. [4] was performed in the framework of the phenomenological Lagrangian model with the Breit-Wigner shape Δ propagator. Therefore we start from

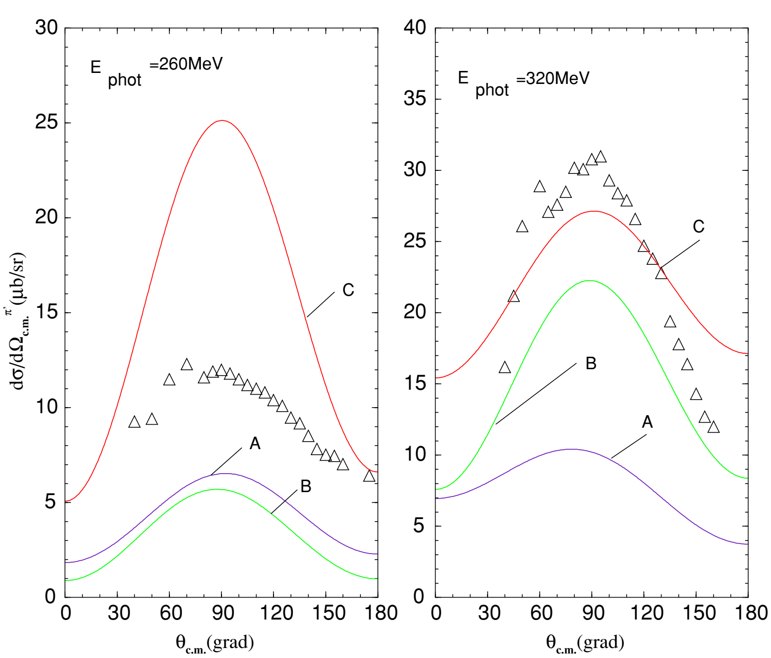

FIG. 11. (Color online) The differential cross sections for the pionphotoproduction reaction for the A [Eq. (27)], B [Eq. (29)], and C [Eq. (33)] Δ propagators. The experimental results indicated by triangles are from Ref. [36].

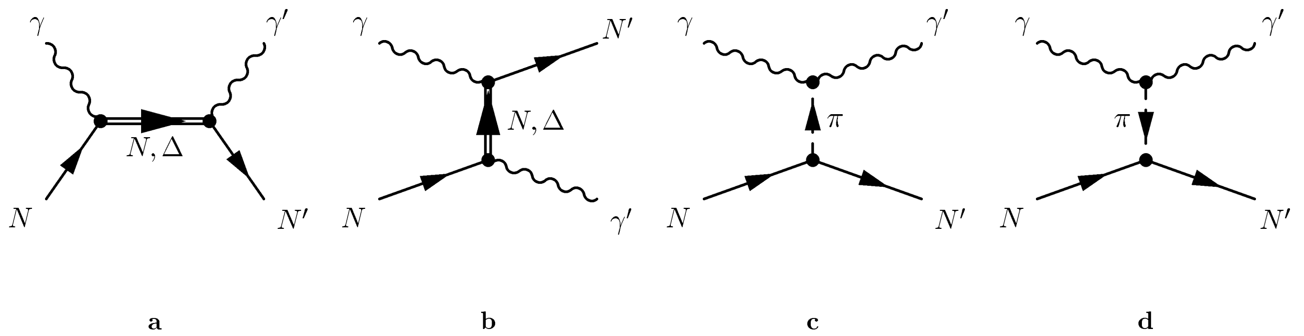

FIG. 12. Diagrams used for the calculation of the Compton scattering $\gamma p \to \gamma' p'$ in the Δ resonance region: (**a**) N, Δ-exchange s-channel terms, (**b**) u-channel terms, and (**c** and **d**) the t-channel π^o exchange diagrams with the different chronological sequence of the intermediate pion emission and absorption. In the "old fashioned" perturbation theory the sum of diagrams **c** and **d** is equivalent to the Feynman one-π-meson-exchange diagram.

model B with the Breit-Wigner type propagator, and we fulfill a following approximations:

(i) First we omit the u-channel Δ-exchange diagram in Fig. 6(b), the ρ-meson exchange diagram in Figs. 6(c), and 6(d) and we will omit the electric and charged parts of the $\gamma N - \Delta$ vertex function [Eq. (A1)]. Then we obtain the curve B' from the curve $B_{\rm born}$, which is identical to the curve B in Fig. 9.

(ii) Next we replace the Δ pole position (i.e., we take $E_r = 1210\,\mathrm{MeV}$ and $\Gamma_\Delta = 100\,\mathrm{MeV}$ as in Ref. [4]). As result the curve B' transforms into $B_{\rm sh}$).

(iii) In the last stage we replace all form factors with the corresponding tree approximation and we use the model

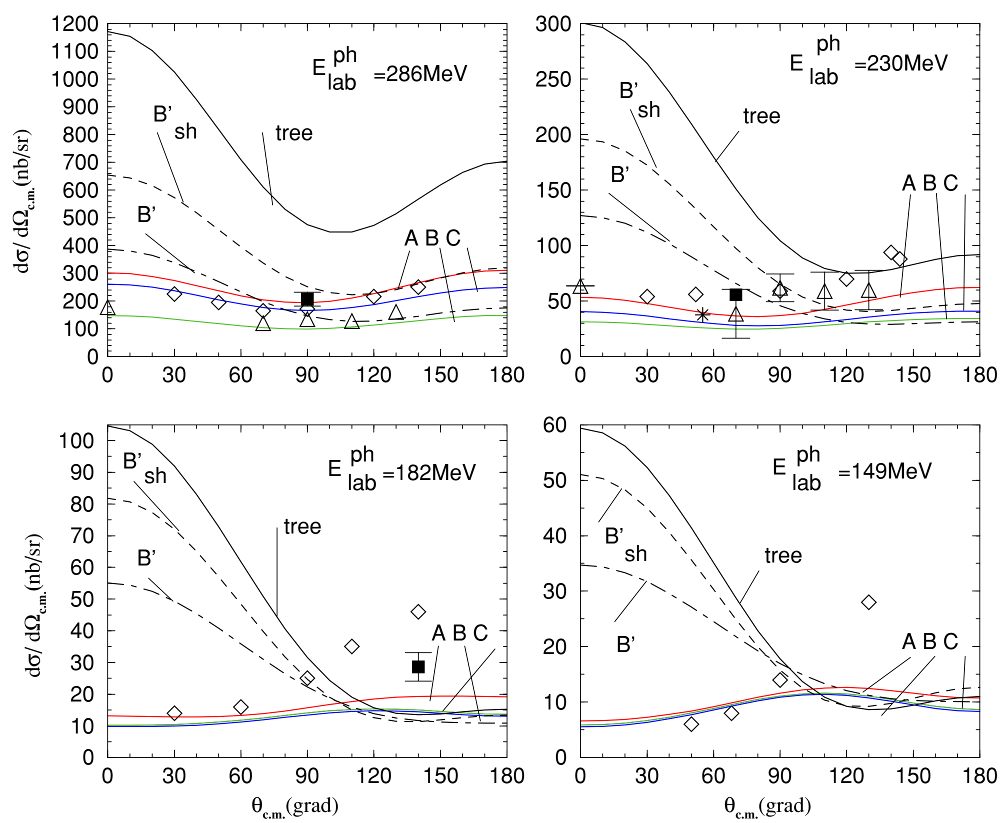

FIG. 13. (Color online) Variation of the differential cross section of the proton Compton scattering reaction for the different propagators of the Δ^+. Curves A, B, and C relate to the expression of the Δ^+ propagator [Eqs. (27), (29), and (33)]. The data are from Ref. [35]. Curve B' is obtained after neglection of the Δ exchange crossing term from the calculations with the Breit-Wigner propagator (model B). The same calculations as for the curve B', but with the shifted parameters of the Δ resonance position, are presented by curve $B'_{\rm sh}$. The curves with the label *tree* denote the calculations in the tree approximation of the vertex function and in the same model of the s-channel Δ exchange term as in Fig. 10.

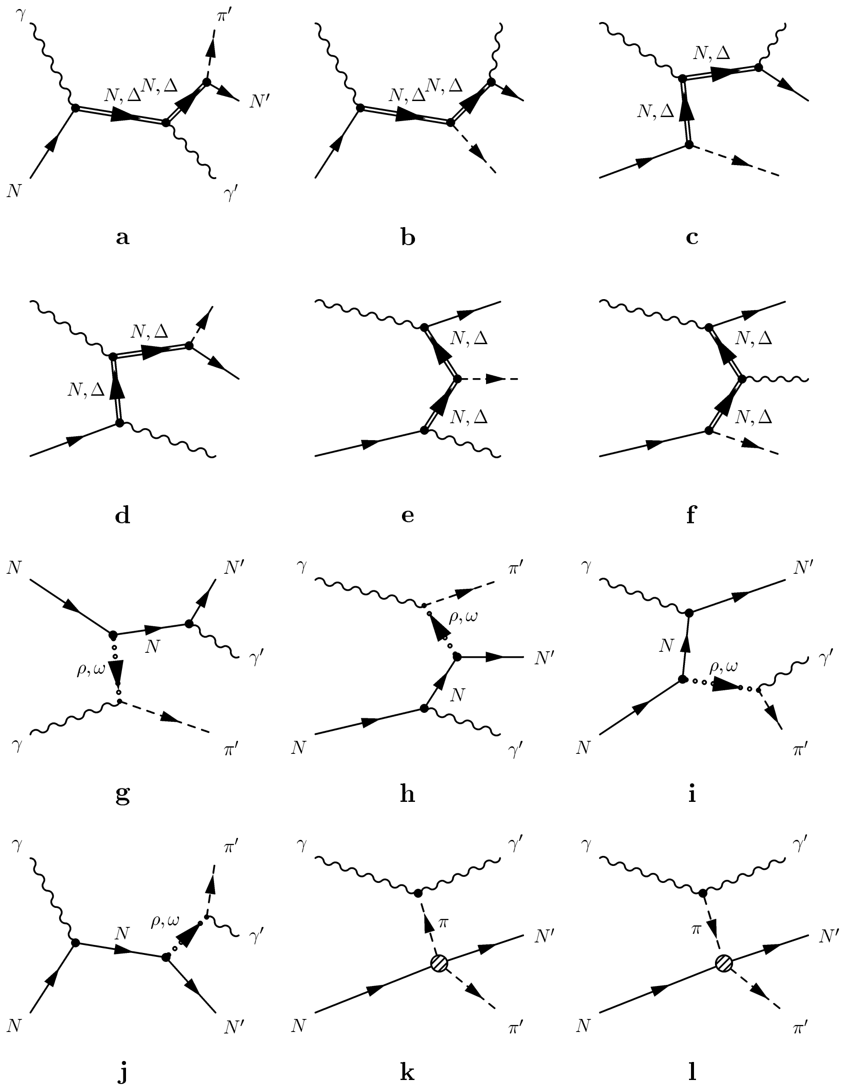

FIG. 14. Diagrams for the $\gamma p \to \gamma' \pi^{o\prime} p'$ reaction with one-particle N, Δ and π^o, ρ, ω exchange that are taken into account in our numerical calculation. For diagrams **b** and **e** contributions of the π-meson creation from the intermediate N or Δ in the transitions (N, N), (N, Δ), and (Δ, N) are included, but not the π^o creation in the (Δ, Δ) transition. In Ref. [38] it is shown that this contribution is weak. In the ρ-, ω-meson exchange diagrams **g**, **h**, **i**, and **j** only nucleon but not the Δ exchange is taken into account. In the one-π^o-exchange diagrams **k** and **l** the dashed circle indicates the πN scattering t matrix.

of the current conservation condition from Ref. [18,4] with the intermediate s-channel N, Δ states. Then curve $B_{\rm sh}$ transforms into the curve labeled as *tree*, which has the same form as the resulting cross section calculated in Ref. [4] and with all these approximations agrees nicely with the data quoted in Ref. [4].

It is well known [9] that the three-body models of the πd scattering cross sections are much less sensitive ($\sim$15–25%) to the choice of the separable model of the πN interaction as the present calculation of the $\gamma p \to \pi^o p$ cross sections. This sufficient sensitivity of the $\gamma p \to \pi^{o\prime} p'$ reaction can be explained by the different scale of the considered amplitudes. Thus the $\pi N - \pi' N'$ cross section is given in mb, the $\gamma N - \pi' N'$ cross section is determined in μb and the scale of the $\gamma p \to \gamma' p'$ and $\gamma p \to \gamma' \pi^{o\prime} p'$ cross sections is determined in nb. Therefore the relative small difference between the πN phase shifts or cross sections can generate a large difference for the calculated $\gamma p \to \gamma' p'$ and $\gamma p \to \gamma' \pi^{o\prime} p'$ cross sections. In addition, the three-body equations for the $\pi d - \pi NN$ scattering reactions contain the whole πN amplitude [Eq. (17a)] in opposite to the $\gamma p \to \pi^{o\prime} p'$ scattering amplitude [Eq. (37)], where the form factor $g_{\Delta-\pi N}(\mathbf{p})$ from the complete πN amplitude [Eq. (17a)] is absent. Therefore in the scale invariance of the separable πN amplitudes in Eq. (37) is broken twice: first by the normalization condition of the Δ propagator [Eqs. (13a) and (13b)] and second because of absence of $g_{\Delta-\pi N}(\mathbf{p}')$ in Eq. (37).

The four-momentum transfer t is small in the low and intermediate energy region. Therefore one can ask the question: why was it important to take into account the vertex functions in the Born approximation from the numerical point of view?

To answer this question, let us consider the usual γN vertex function

$$\langle \mathbf{p}'_N | J_\mu(0) | \mathbf{p}_N \rangle = \overline{u}(\mathbf{p}'_N) \left[\gamma_\mu F_1(t) + i \frac{g_M}{2m_N} \sigma_{\mu\nu} (p'_N - p_N)^\nu F_2(t) \right] u(\mathbf{p}_N). \tag{38}$$

In the tree approximation $F_{1,2}(t) = 1$ and $E_{\mathbf{p}'_N} - E_{\mathbf{p}_N}$ is replaced by k_γ. For $k_\gamma \simeq 350$–450 MeV t is small and $F_{1,2}(t) \approx 0.9$–0.96 but $E_{\mathbf{p}'_N} - E_{\mathbf{p}_N} \simeq 40$–$50$ MeV. Thus

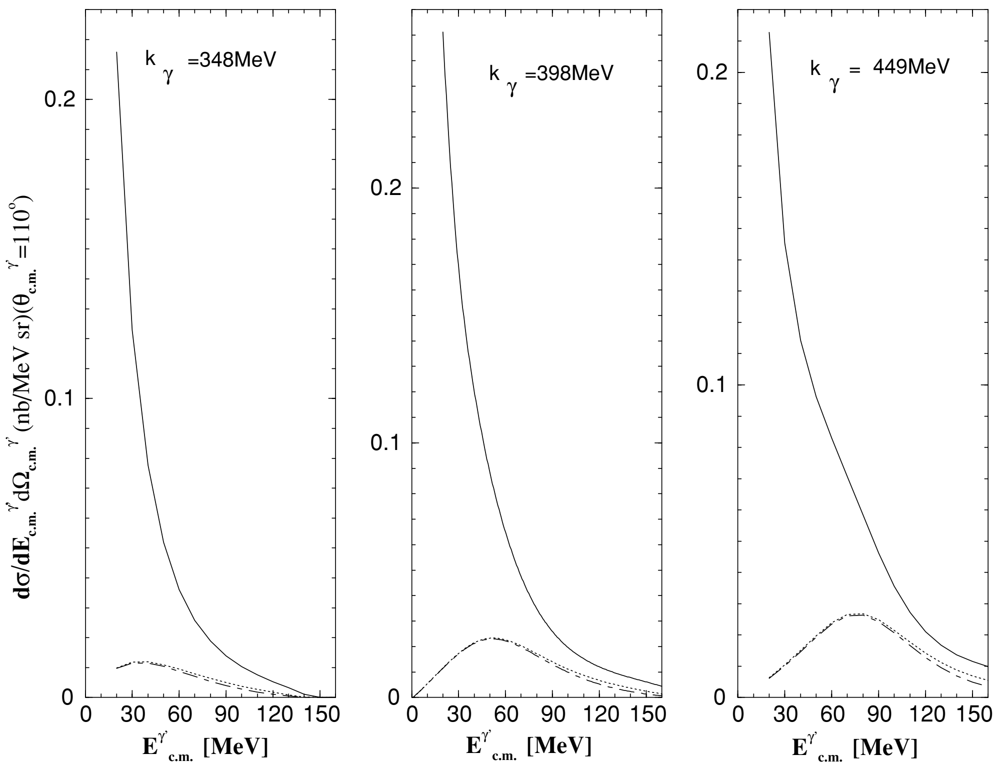

FIG. 15. Cross section $d\sigma/dE_{\gamma'}d\Omega^{\gamma'}_{\text{c.m.}}[nb/\text{MeV}sr]$ of the $\gamma p \to \gamma'\pi^{o\prime}p'$ reaction with the Δ propagator of the Breit-Wigner shape [Eq. (29)] and for different energies of the incoming photon $|\mathbf{k}_\gamma| \equiv E_\gamma$. The dashed line corresponds to our calculation without $p-\gamma'p'$ or $p'-\gamma'p$. The long-dashed line is our result with only the diagram with the $\Delta-\gamma'\Delta'$ transition. The full curve includes the contributions of all diagrams in Fig. 14.

the difference between the zero component of the vertex function [Eq. (38)] and the same vertex function in the tree approximation may be great enough. This difference is larger for the $\gamma N\Delta$ vertex [31] [Eq. (A.1)] than for the γN vertex function (3.9). Therefore we see that the kinematical structure of the magnetic part of the vertex functions can generate the essential difference between the cross sections calculated in the tree and in the Born approximations.

The differential cross section of the $\gamma p \to \pi^{o\prime}p'$ reaction for the two energies ($E^{\gamma}_{\text{lab}} = 260, 320\,\text{MeV}$) are depicted in Fig. 11 with models A, B, and C of the Δ isobar propagators. As in the case for the integral cross sections in Fig. 9, the curves with the different Δ propagators in Fig. 11 differ greatly and no one is preferable for description of the experimental observables.

B. Compton scattering on the proton

We consider the elastic γp scattering reaction in the Δ resonance region in the Born approximation using the diagrams depicted in Fig. 12. Diagrams **a** and **b** in Fig. 12 correspond to the $\gamma p \to \gamma' p'$ reaction in the s and u channels with intermediate N and Δ states. Diagrams **c** and **d** show the one-π^o-exchange interaction in the elastic γp scattering reaction. The calculation of the proton Compton scattering in Ref. [7] was based on the same diagrams, but it was performed in the framework of the tree approximation.

Figure 13 shows the differential cross section for the elastic Compton scattering reaction on the proton with the different energies of the incoming photon ($E^{\text{ph}}_{\text{lab}} = 149, 182, 230,$ and $286\,\text{MeV}$) and with the different Δ isobar propagators. The sensitivity of these cross sections to the form of the Δ propagators increases in the Δ resonance region. To continue the comparison of our calculation with the calculations in the tree approximation we fulfill the same set of approximations as for the case of the π^o photoproduction reaction. We start from the Breit-Wigner shape model for the Δ propagator and on the first stage we omit the contributions from the u channel Δ exchange term [Fig. 12(b)]. After this we obtain the curve B'. The same calculation with the shifted values of the Δ pole parameters $m_\Delta = 1210\,\text{MeV}$ and $\Gamma_\Delta = 100\,\text{MeV}$ gives us the curve B'_{sh}. The curve labeled *tree* results after the use of the tree approximation of the all vertex functions using the model of the Δ propagator with the corresponding model of the current conservation [18].

The difference between the curves B, B', B'_{sh}, and *tree* indicates the importance of the above approximations also for the proton Compton scattering reaction. Moreover, from the comparison of the calculations with the three different models of the Δ propagator (A [Eq. (27)], B [(29)], and C [Eq. (33)]), it is seen that non among these calculations are preferable with respect to the experimental data [35]. We note that the approximations indicated as B', B'_{sh}, and *tree* (i.e., the

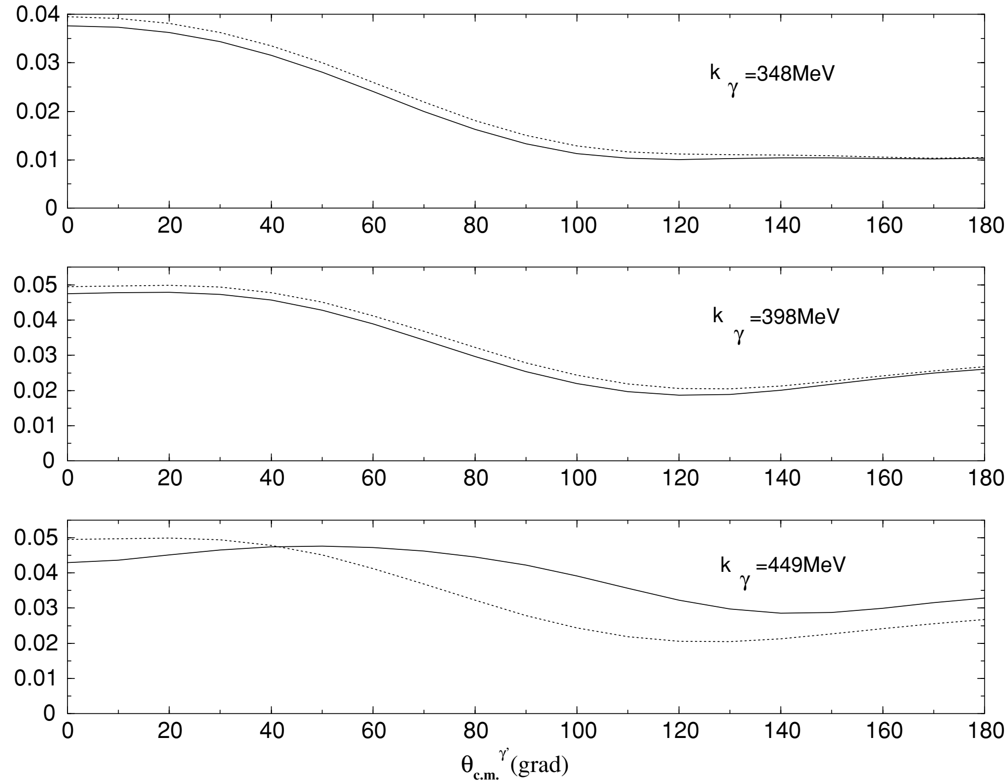

FIG. 16. $d\sigma/d\Omega^{\gamma'}_{\text{c.m.}}[nb/sr]$ cross section of the $\gamma p \rightarrow \gamma'\pi^{o\prime}p'$ reaction with the averaged energy of the emitted photon 30 MeV $< E^{\gamma'}_{\text{c.m.}} <$ 130 MeV and variations of the final photon angle. The dotted line by the $\theta^{\gamma'}_{[\text{c.m.}]} = 0$ grad corresponds to $\mu_\Delta = 2.79\,\mu_N$ and solid line relates to $\mu_\Delta = 2 \times 2.79\,\mu_N$.

approximations used in Refs. [4,18]) generate a description worse for these data than for the pion photoproduction reaction.

C. The $\gamma p \rightarrow \gamma'\pi^{o\prime}p'$ reaction

We have calculated the $\gamma p \rightarrow \gamma'\pi^{o\prime}p'$ reaction with the same vertex functions as the $\gamma p \rightarrow \gamma' p'$ and $\gamma p \rightarrow \pi^{o\prime}p'$ reactions (see the appendix). This calculation includes the $4 \times 6 = 24$ N, Δ exchange diagrams **a–f** in Fig. 14. That is the complete set of the one-particle N, Δ-exchange diagrams that arise in the three-dimensional time-ordered formulation with the double N, Δ-exchange interaction. We have omitted the meson $\Delta - \Delta$ and heavy − meson $N - \Delta$ couplings. Therefore in the next four diagrams (**g–j**) in Fig. 14 we have only one-nucleon exchange contributions. Two last diagrams with one-π^o-exchange term (**k** and $\boldsymbol{\ell}$) are important for the $\gamma p \rightarrow \gamma' p'$ reaction. The πN scattering t matrix in the **k** and **1** is approximated by the N, Δ-exchange s, u-channel terms. Because of the small π^o decay coupling constant [see Eq. (A9) in the appendix], contributions of the π^o exchange diagrams (**k** and $\boldsymbol{\ell}$) are small (less than 1% in our calculation of the corresponding cross section).

The goal of our calculation of the reaction $\gamma p \rightarrow \gamma'\pi^{o\prime}p'$ is to estimate the contributions of the background diagrams that are mixed with the double-Δ exchange diagram with the $\Delta - \Delta'\gamma'$ transition (diagram **a** in Fig. 14). This diagram contains the interesting value of the Δ^+ magnetic moment μ_Δ [see Eq. (A.7) in the appendix) and gives the most important contribution for the determination of the magnetic moment of the Δ^+ resonance. An other diagram with a $\Delta\gamma - \Delta'$ transition is depicted in **c**, **d**, and **f**. Nevertheless the contribution of these diagrams is not large, only *a few percentages*. The complete number of the calculated diagrams is 38 (24 diagrams in **a–d**, −2 diagrams with the $\Delta - \pi\Delta$ coupling in **b** and **e** $2 \times 4 = 8$ diagrams in **g–j**, and 2 diagrams in **k** and $\boldsymbol{\ell}$ with s-, u-channel N, Δ exchange instead of the πN interaction; $4 \times 6 - 2 + 2 \times 4 + 2 \times 4 = 38$).

To separate the contribution of the double Δ-exchange diagrams (**a** in Fig. 14) with the $\Delta - \Delta\gamma'$ vertex we have first to separate the contributions of the diagrams that have the infrared singularity for the emitted slow final photons when $E_{\mathbf{k}'_\gamma} = |\mathbf{k}'_\gamma| \rightarrow 0$. This singularity arises in the intermediate proton propagator at the $p'' - \gamma' p$ vertex function. All diagrams in Fig. 14 except the last four diagrams contains the $p'' - \gamma' p$ transition. These diagrams generate a $1/E_{\gamma'}$ energy dependence behavior in the cross sections of the bremsstrahlung reactions. The terms with the $\Delta'' - \gamma'\Delta$ transitions in Figs. 14(a) and 14(f) have the Δ propagators (see Eq. (6) in Ref. [2]) $[E_{p'_N} + E_{p'_\pi} - E_{\mathbf{p}_\Delta} - \Sigma_{\pi N}(E, \mathbf{p}_\Delta)]^{-1}$ and $[E_{k'_\gamma} + E_{p'_N} + E_{p'_\pi} - E_{\mathbf{p}_\Delta} - \Sigma_{\pi N}(E, \mathbf{p}_\Delta)]^{-1}$ with real energies and complex $\Sigma_{\pi N}(E, \mathbf{p}_\Delta)$. Therefore the Δ propagators at the $\Delta'' - \gamma'\Delta$ transitions are free from the infrared singularity. In the calculation of the $\gamma p \rightarrow \gamma'\pi^{o\prime}p'$ reaction in the framework of the effective Lagrangian method with

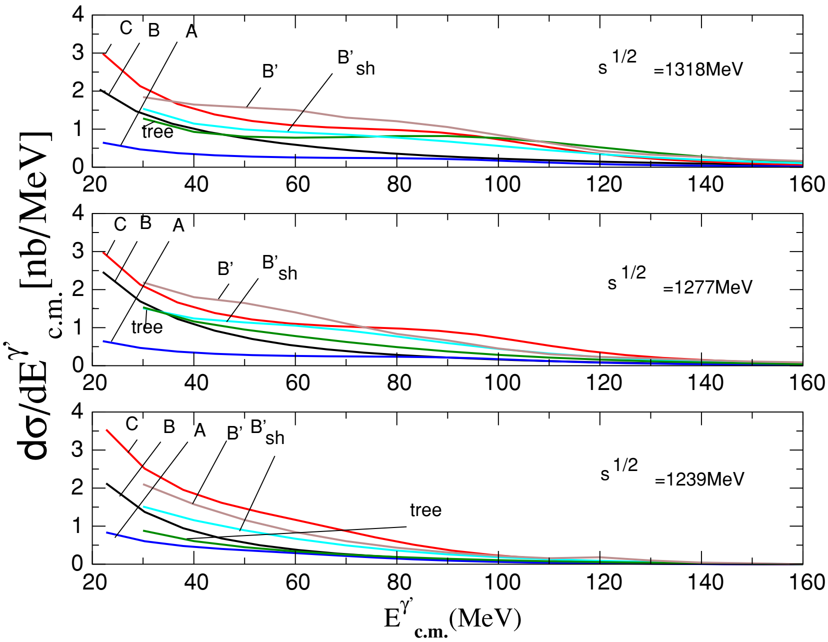

FIG. 17. (Color online) Cross section $d\sigma/dE^{\gamma'}{}_{\text{c.m.}}[nb/\text{MeV}]$ as function of the energy of the emitted photon γ' for the incident photon energies $E_\gamma = 348$, 398, and 449 MeV and for the different Δ propagators A [Eq. (27)], B [Eq. (29)], and C [Eq. (33)]. Curves B', B_{sh}, and *tree* denote the calculations with the same modifications of the Breit-Wigner shape propagator as in Fig. 10. For the magnetic moment $\mu_{\Delta^+} = 2.79$ [nuclear magnetons] has been assumed.

the Feynman diagrams in the tree approximation [4] the Δ-propagators at the $\Delta - \gamma'\Delta$ vertex are also free from the infrared singularity. The set of diagrams in Fig. 14 includes all of possible infrared singularities generated from the emission of final photon from the external protons. Only diagram **a** in Fig. 14 corresponds to the emission of γ' from the internal protons. To take into account the complete set of the internal mechanisms of the emission of the low-energy final

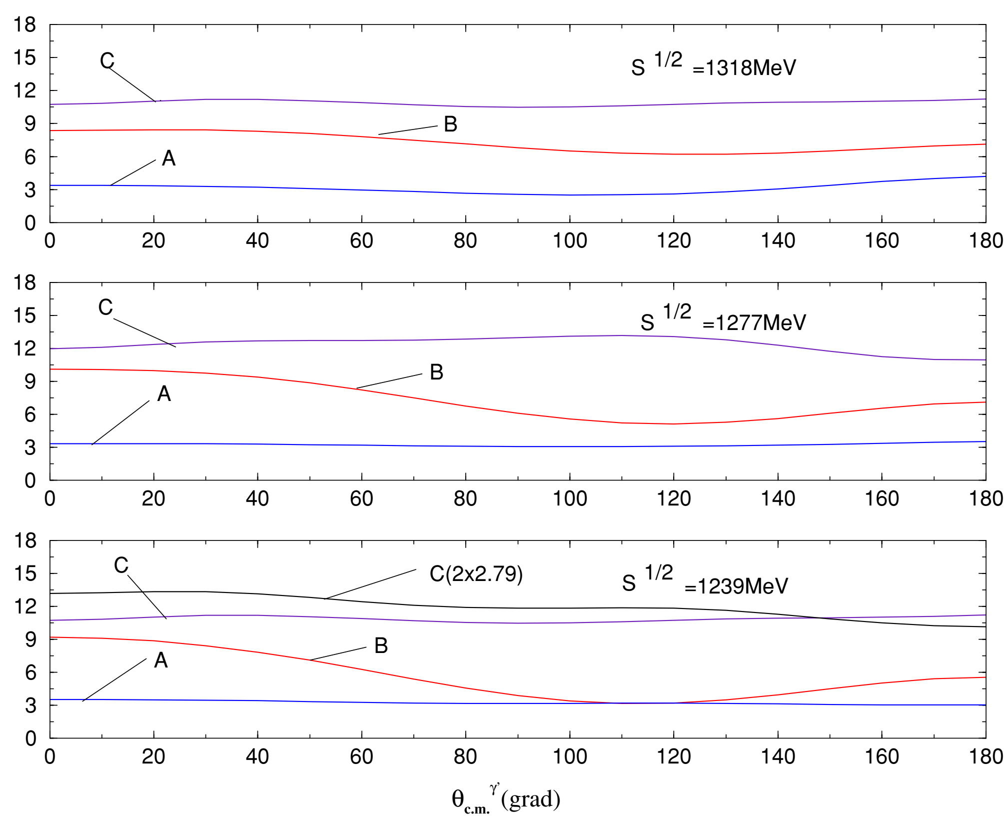

FIG. 18. (Color online) Angular distribution $d\sigma/d\Omega^{\gamma'}{}_{\text{c.m.}}[nb/sr]$ of the final photon γ' with the averaged final photon momentum 30 MeV $< E^{\gamma'}_{\text{c.m.}} < 130$ MeV. The different curves represent the three different approaches for the Δ propagator and three different initial photon energies as in the previous figure. For $s^{1/2} = 1239$ MeV and Δ propagator of model C [Eq. (33)] the angular distribution of the emitted γ' is calculated for two magnetic moments (2.79 and 2 × 2.79) [nuclear magnetons] of the Δ^+ resonance.

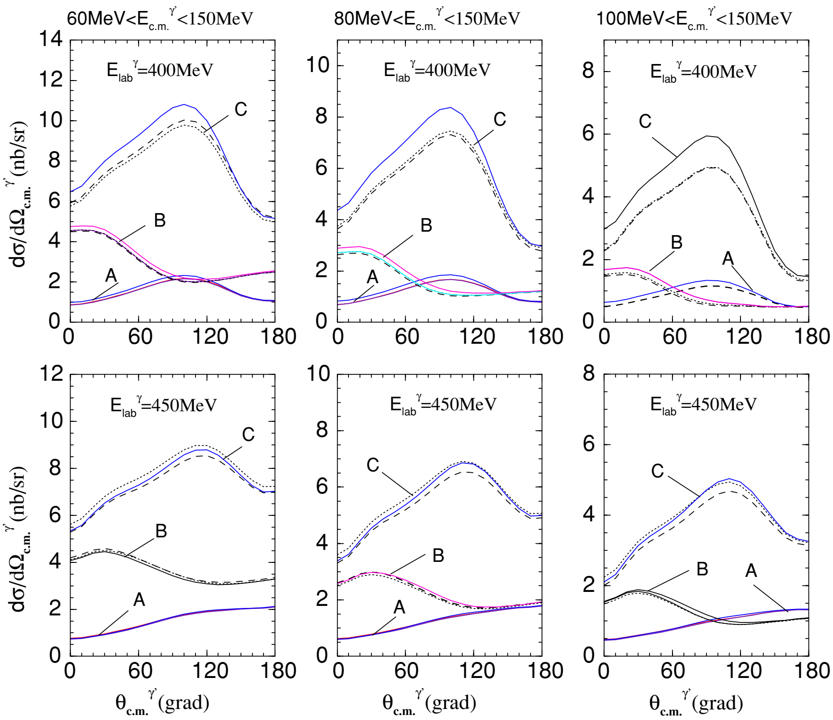

FIG. 19. (Color online) Variation of the angular distribution $d\sigma/d\Omega^{\gamma'}_{\rm c.m.}[nb/sr]$ of the final photon γ'energies, for different energies of the initial photon γ, for different propagators of the Δ (A, B, and C; see text) and for different values of the magnetic moments of the Δ^+. The dashed line corresponds to $\mu_\Delta = 0$. The full curve for the values $\mu_\Delta = 3$, μ_N and dotted line relates to the $\mu_\Delta = 6\,\mu_N$. The energies of the final photons $E^{\gamma'}_{\rm c.m.}$ are integrated over different intervals: $60 < E^{\gamma'}_{\rm c.m.} < 150$ MeV, $80 < E^{\gamma'}_{\rm c.m.} < 150$ MeV, and $100 < E^{\gamma'}_{\rm c.m.} < 150$ MeV for two initial photon energies: $E^{\gamma}{}_{\rm lab} = 400$ MeV and $E^{\gamma}{}_{\rm lab} = 450$ MeV.

photons it is necessary to include the complete form of the two-body $\pi N - \gamma N$ and $\gamma N - \gamma N$ amplitudes in equations for the three-body $\gamma N - \gamma\pi N$ amplitudes as is done in Ref. [10].

To estimate the contribution of the diagrams with infrared singularities at the $N - \gamma' N$ transition in Fig. 14, we consider Fig. 15, where the cross sections $d\sigma/dE_{\gamma'}d\Omega^{\gamma'}_{\rm c.m.}$ with $E^{\rm lab}_{\gamma} = 348, 398,$ and 449 MeV, $\theta^{\gamma'}_{\rm c.m.} = 110$ grad; $\phi^{\gamma'}_{\rm c.m.} = 0$ with the Breit-Wigner type propagator [model B, Eq. (29)] are shown. The full curve includes the contributions of all diagrams from Fig.14, the dashed curve corresponds to the contribution of the single diagram with the $\Delta - \gamma'\Delta$ transition [Fig. 14(a) with the intermediate $\Delta' s$] and the long-dashed curve includes the contributions of all diagrams without the infrared $p - \gamma' p'$ transition. From Fig. 15 we see, that the contribution of the interesting double-Δ-exchange diagram (**a** from Fig. 14) is comparable with the contributions of all other diagrams only after 80 MeV of the energy of the emitted photon (i.e., when $E^{\rm c.m.}_{\gamma'} \simeq 80$ MeV). The contribution of this diagram is further increased by

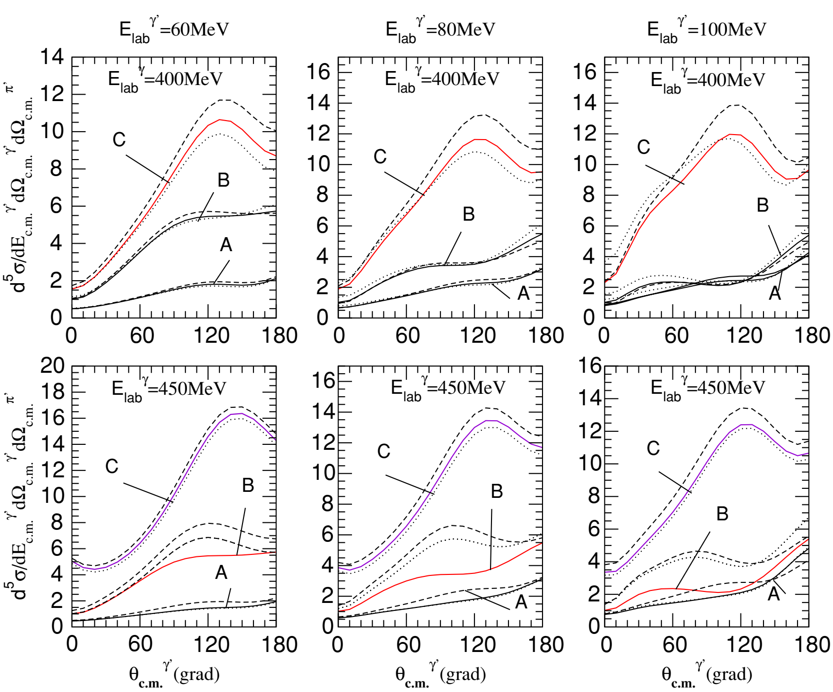

FIG. 20. (Color online) Angular distribution for the fivefold cross section $d^5\sigma/dE^{\gamma'}_{\rm c.m.}d\Omega^{\gamma'}_{\rm c.m.}d\Omega^{\pi'}_{\rm c.m.}[nb/{\rm GeV}sr^2]$ for the following angles of the final photon and pion $\phi_{\gamma'} = 0^\circ$, $\theta^{\pi'}{}_{\rm lab} = 15^\circ$ and $\phi_{\pi'} = 0^\circ$.

increasing of the energy of the initial photon. The major contributions of diagram **a** with the $\Delta \to \Delta'\gamma'$ vertex function were observed for the following direction of the emitted photon $\theta^{\gamma'}_{\rm c.m.} = 110$ grad; $\phi^{\gamma'}_{\rm c.m.} = 0$. Therefore the most preferable kinematical region for the investigation of the role of the $\Delta - \gamma'\Delta$ transition in the $\gamma p \to \gamma'\pi^{o\prime}p'$ reaction is $E^{\rm c.m.}_{\gamma'} >$ 80 MeV and $\theta^{\gamma'}_{\rm c.m.} \sim 110$ grad; $\phi^{\gamma'}_{\rm c.m.} \sim 0$ grad.

In Fig. 16 the same cross sections as in Fig. 15 are displayed but with different $\mu_\Delta = 2.79\,\mu_N$ and $\mu_\Delta = 2 \times 2.79\,\mu_N$ magnetic moments of the Δ^+ resonance. The difference between corresponding curves by $E^{\rm lab}_\gamma = 348$ and 398 MeV is quantitative and roughly no more than 10%. But for the $E^{\rm lab}_\gamma = 449$ MeV this difference is more significant.

In Fig. 17 and 18 the cross sections $d\sigma/dE^{\gamma\prime}{}_{\rm c.m.}$ and $d\sigma/d\Omega^{\gamma'}{}_{\rm c.m.}$ for different energies of the initial photon ($E^{\rm lab}_\gamma =$ 348, 398, and 449 MeV corresponds to $s^{1/2} = 1239, 1277$, and 1318 MeV) and with the different Δ propagators from models A, B, and C of Sec. V are depicted. The difference between corresponding curves is large and, most important, in the small emitted photon region (i.e., the sensitivity of the amplitude of the $\gamma p - \gamma'\pi'^{o}p'$ reaction on the form of the Δ propagator is larger for the small $E'_{\rm c.m.}$). Unfortunately, the sensitivity of these curves on the different values of the Δ^+ magnetic moment is small (<10%). The exception is in Fig. 14 for the total energy $s^{1/2} = 1239$ MeV corresponding to $E^\gamma{}_{\rm lab} = 348$ MeV, where the Δ propagator of model C [Eq. (33)] was used for magnetic moments $\mu_{\Delta^+} = 2.79$ and 2×2.79 [nuclear magnetons].

The curves in Fig. 17 and in Fig.18 qualitatively describe the preliminary experimental data that has been measured by the A2/TAPS collaboration at MAMI [5]. The sensitivity of the calculated cross section $d\sigma/dE^{\gamma\prime}{}_{\rm c.m.}$ and $d\sigma/d\Omega^{\gamma'}{}_{\rm c.m.}$ on the magnitude of the Δ^+ magnetic moment is even smaller as in the corresponding calculation in Ref. [2,4]. This difference can be explained different gauge conditions, different number of included diagrams, different vertex functions, and so on. Only more complete calculations of the multichannel γp scattering equations with unitarity and a more consistent model of the Δ propagator, with rescattering effects in the nonresonant πN interactions and antinucleon degrees of freedom can quantitative determine the interesting differential cross sections. Keeping in mind that the cross sections of the $\gamma p \to \gamma'\pi^{o\prime}p'$ reaction are more sensitive to the form of the Δ particle propagator as to the magnitude of the Δ^+ resonance, the following question appears: is the present sensitivity of these differential cross sections enough for determination of the magnetic moment of the Δ^+ resonance? Or, in other words, does a kinematical region exist where results of our calculation qualitatively depend on μ_{Δ^+}? To find the kinematical region where the the dependence on μ_Δ is sufficient, we consider the following cross sections.

In Fig. 19 the sensitivity of the angular distribution $d\sigma/d\Omega^{\gamma'}_{\rm c.m.}$ for model A [Eq. (27)], B [Eq. (29)], and C [Eq. (33)] of the Δ propagators with three different magnitudes of the Δ^+ magnetic moment $\mu_{\Delta^+} = 0, 3\mu_N, 6\mu_N$ is demonstrated. Calculations are performed for two values of the initial photon energy $E^\gamma{}_{\rm lab} = 400$ and 450 MeV, where the energies of final photon are integrated over the following intervals: $80 < E^{\gamma'}_{\rm c.m.} < 150$ MeV and $100 < E^{\gamma'}_{\rm c.m.} < 150$ MeV. For $E^\gamma{}_{\rm lab} = 400$ MeV the variation of μ_{Δ^+} gives an essential difference of about ∼20%, for model C of the Δ propagator. This difference decreases for $E^\gamma{}_{\rm lab} = 450$ MeV. In this case the cross sections for the $\mu_{\Delta^+} = 0$ and $3\mu_N$ practically coincide. This is different in the case with $E^\gamma{}_{\rm lab} = 400$ MeV, where the curves with $\mu_{\Delta^+} = 0$ and $6\mu_N$ are close to each other. But one obtains a different result for $\mu_{\Delta^+} = 3\mu_N$. The values of the cross section with the propagators A and B are close to the experimental data [5], but these curves are less dependent on μ_{Δ^+}. In addition the behavior of cross sections A are quantitatively different for the $E^\gamma{}_{\rm lab} = 400$ MeV and for the $E^\gamma{}_{\rm lab} = 450$ MeV.

The sensitivity of the cross sections to different models of Δ propagators and to the Δ^+ magnetic moments $\mu_{\Delta^+} = 0, 3\mu_N, 6\mu_N$ is examined also in Fig. 20, where the five fold cross sections $d^5\sigma/d^3{\bf k}'^{\gamma'}_{\rm c.m.}d\Omega^{\pi'}_{\rm c.m.}$ with fixed values of the scattering angles $\phi_{\gamma'}, \theta^{\pi'}{}_{\rm lab}, \phi_{\pi'}$ and the emitted photon energy are shown. Unlike in the previous figure, here the difference between the curves with different μ_N is more visible. Most promising is the quantitative difference between differential cross sections for the model B with $E^\gamma{}_{\rm lab} = 450$ MeV and $\mu_{\Delta^+} = 0$, $\mu_{\Delta^+} = 3\mu_N$ and $\mu_{\Delta^+} = 6\mu_N$. This difference is not only very large, but also quantitatively different as for the incident photon energy $E^\gamma{}_{\rm lab} = 400$ MeV.

Thus we see that in special kinematical regions the sensitivity of differential cross sections of the $\gamma p \to \gamma'\pi^{o\prime}p'$ reaction to the magnitude μ_{Δ^+} can be large and this difference can have a qualitative nature. The corresponding kinematical region is different for the different Δ propagators. But the region with the $E^\gamma{}_{\rm lab} > 400$ MeV, $E^{\gamma'}{}_{\rm lab} > 80$ MeV, and $\theta^{\gamma'}{}_{\rm c.m.} \simeq 110^\circ$ is most preferable for the determination of the Δ^+ magnetic moment μ_{Δ^+}.

VII. CONCLUSION

In the present article we consider the possibility of extracting the Δ magnetic moment in the $\gamma p \to \pi^{o\prime}p'$ reaction. Our calculations are performed in the Born approximation using the complete set of one-particle $N, \Delta, \pi, \rho, \omega$-exchange diagrams in the time-ordered field-theoretical approach. In this formulation the intermediate Δ propagator is on mass shell and we examine different models for the Δ propagators. These propagators are obtained from two different unitary separable models of the πN scattering amplitude and from the tree-level model of the relativistic Breit-Wigner shape representation of the πN amplitude that does not satisfy the unitarity condition. It is well known that the one-Δ exchange model reproduces well the πN scattering data in the Δ resonance region. Therefore the difference in the description of the multichannel γp reactions with the different on shell Δ propagators can be explained only by the different description of the πN scattering data in the Δ resonance region. The corresponding descriptions of the π^+p scattering data for the applied models of the Δ propagators are demonstrated in Fig. 6 and in Fig. 7.

The main result of our work is that the numerical description of the coupled $\gamma p \to \pi^{o\prime}p'$, $\gamma p \to \gamma'p'$, and $\gamma p \to \gamma'\pi^{o\prime}p'$ reactions in the Δ-resonance region is very sensitive to the model of the on mass shell Δ-propagator. From this result follow conclusions:

(i) The use of the relativistic Breit-Wigner shape Δ propagator with the nonunitary representation of the πN amplitude for the calculation of the coupled $\gamma p \to \pi N$ and $\gamma p \to \gamma\pi^o p$ reactions is inconsistent because this nonunitary model gives a nonrealistic description of the leading πN scattering amplitude.[1]

(ii) The relatively small difference in millibarn (mb) by description of the leading πN scattering cross section with two Δ propagators can generate the large difference between the calculated $\gamma p - \pi^o p$ cross sections in microbarn (μb) and for the $\gamma p - \gamma\pi^o p$ cross sections in nanobarn (nb).

(iii) In order to fix the form of the on shell Δ propagator it is necessary to achieve a unified description of the $\pi N \Longleftrightarrow \gamma N \Longleftrightarrow \pi\pi N$ reactions together with the weak $\gamma p - \gamma'\pi' N'$ channel.

(iv) The unified description of the $\pi N \Longleftrightarrow \gamma N \Longleftrightarrow \pi\pi N$ reactions together with the $\gamma p - \gamma'\pi' N'$ channel implies the determination of the sought value of the Δ^+ magnetic momenta.

It must be noted that the other kind of the large sensitivity of the observables of the πN and γp elastic scattering on the off shell behavior of the microscopic Δ propagator was also indicated in the papers [8,7].

Despite of the strong dependence of the calculated cross sections on the Δ propagators, one can indicate the most convenient kinematical region for the determination of the magnetic moment of the Δ^+-resonance with any considered model of the Δ propagator. For instance, from Fig. 15 it is seen that the contributions of the interesting $\Delta \to \gamma'\Delta'$ vertex can be extracted in the region $E^{\rm cm}_{\gamma'} > 80\,{\rm MeV}$ and $\theta^{\gamma'}_{\rm cm} \sim 110^\circ; \phi^{\gamma'}_{\rm cm} \sim 0^\circ$.

The sensitivity of the cross section of the $\gamma p \to \gamma'\pi^{o\prime} p'$ reaction to the different values of the Δ^+ magnetic moment μ_{Δ^+} is unfortunately smaller then the dependence of these cross section on the model of the Δ propagator. Thus the sensitivity of most differential cross sections is less than 10% if the magnetic factor changes by a factor of 2. However, it was demonstrated (see Figs. 19 and 20) that for every Δ propagator one can find a special kinematical region, where differences between calculated cross sections with different μ_{Δ^+} are qualitative or yield an effect of more than 25%. These findings make it possible to extract in the future with more improved calculations of the magnitude of the μ_{Δ^+} from the experimental data of the $\gamma p \to \gamma'\pi^{o\prime} p'$ reaction. Certainly, for this aim it is necessary to solve more general three-body field-theoretical equations for the coupled $\pi N \longleftrightarrow \pi\pi N \longleftrightarrow \gamma N \longleftrightarrow \gamma\pi N$ amplitudes which satisfy the three-body unitarity condition [10]. Therefore the present work can be considered a preliminary investigation of the preliminary experimental data of the $\gamma p \to \gamma'\pi^{o\prime} p'$ reaction [5].

It was shown that, starting from our calculations with the Breit-Wigner propagator for the Δ resonance, after performing the additional set of approximations and redefinitions of parameters, we reproduce exactly the tree-level calculation done in Ref. [4] for the $\gamma p \to \gamma'\pi^{o\prime} p'$ and the $\gamma p \to \pi' N'$ reactions. These result of the tree-level calculations [4] are in good agreement with the preliminary data [5] for the $\gamma p \to \gamma'\pi^{o\prime} p'$ and the $\gamma p \to \pi' N'$ reactions [4]. But as it was noted above, this model is in contradiction with the leading πN scattering data.

Another result of the present work is the recipe of construction of the microscopic propagator of the Δ resonance [Eqs. (16) or (24)] in the framework of the separable model of the πN P_{33} partial amplitude [Eqs. (18a) or (17a)]. Using the relation [Eq. (20)] between the projection operators on the πN P_{33} partial states and the projection operator $u^\mu(\mathbf{p}_\Delta)\overline{u}^\nu(\mathbf{p}_\Delta)$ [Eq. (21a)], we have obtained the relations [Eqs. (26a) and (26b)] between the Δ exchange amplitude [Eq. (17a)] and the πN P_{33} partial amplitude [Eq. (18a)]. The suggested procedure allows us to obtain the microscopic $\pi N \to \Delta$ form factor and the microscopic Δ propagator directly from the πN P_{33} partial-wave phase shifts. The separable representation of the Δ exchange amplitudes for the $\pi N - \pi N$ and $\gamma N - \pi N$ reactions follows from the general analytical structure of these amplitude, which automatically satisfy the unitarity condition.

ACKNOWLEDGMENTS

Authors thank D. Drechsel, M. I. Krivoruchenko, and M. Vanderhaeghen for discussions. We express our gratitude to M. Kotulla and V. Metag for the current interest to this work and for useful remarks. This work is supported by the "Deutsche Forschungsgemeinschaft" under contract 436 GEO 17/3/0-1.

APPENDIX: VERTEX FUNCTIONS

In the considered formulation nucleon and Δ isobar are defined on mass shell (i.e., N and Δ are included only in the

[1]After preparation of the present text new articles about the extraction of the Δ^+ magnetic moment from the $\gamma p \to \gamma'\pi' N'$ reaction [46,47], where the improved version of Ref. [4] was used, were published. Unfortunately in these investigations the pion-nucleon phase shifts were considered also independently from the Breit-Wigner type Δ propagator.

Moreover, these investigations are based on the low energy theorems for the small momentum of the emitted photon. But for the small $k'_\gamma \sim 1 - 10\,{\rm MeV}$ the contribution of the diagram with the interesting $\Delta \to \gamma'\Delta'$ transition is small comparing to the background diagrams with the photon emission from the initial or from the final nucleon (see Fig. 15). On the other hand in the $k'_\gamma \sim 30 - 90\,{\rm MeV}$ region the contributions of diagrams **a**, **b**, and **c** in Fig. 14 with the $\Delta \Longleftrightarrow \gamma' N$ transitions are important beginning from the Born approximation. These diagrams are omitted in the calculations based on the theorems low energy theorems. Therefore the theorems concerning low energy do not work in the experimentally observed energy region $k'_\gamma \sim 30{-}90\,{\rm MeV}$. The same conclusion was given also in Ref. [32].

bracket vector as ordinary one-particle states). Therefore, the three particle vertex functions with nucleons and Δ isobars are depending only on the four-momentum transfer t. In our calculation we have used the following vertex functions:

The $\gamma N - N$ vertex function in the Coulomb gauge is given in Eqs. (8), (10a), and (10b) [11]. The exact form of the formfactors $F_{1,2}(t)$ is considered, for example, in Ref. [39]. In our calculation for the photon-proton vertex function we have taken $F_1(t) = F_2(t) \equiv f(t) = (1 - t/a^2)^{-2}$; $a = 0.249$ fm; $\mu_N = 1.79$.

$\pi N - N$ vertex function is taken from the dispersion relation analysis [13]

$$\langle \mathbf{p}'_N | j_\alpha(0) | \mathbf{p}_N \rangle = iG(t)\overline{u}(\mathbf{p})\gamma_5 \tau_\alpha u(\mathbf{p});$$
$$G(t) = g_{\pi N}\left[1 + \frac{t\left(t - 4m_N^2\right)}{4m_N^2 m_o^2}\right]^{-1} \tag{A.1}$$

where $m_o = 8.6 m_\pi$; $g_{\pi N} = 12.78$.

In the $\gamma N - \Delta$ vertex function of Jones-Scadron [31], p_Δ is the four-vector the spin 3/2 particles with the real mass m_Δ, i.e.,

$$p_\Delta = \left(\sqrt{m_\Delta^2 + \mathbf{p}^2}, \mathbf{p}\right)$$

and

$$\begin{aligned}\langle \mathbf{p}'_N | J^\mu(0) | \mathbf{p}_\Delta \rangle &\equiv \{\langle \mathbf{p}'_N | J^\mu(0)\}_{\pi N\,\text{irreducible}} | \Psi_{\mathbf{p}_\Delta}\rangle \\ &= \overline{u}(\mathbf{p}'_N)\big[F_M(t)\Gamma_M^{\mu\nu}(t) F_E(t)\Gamma_E^{\mu\nu}(t) \\ &\quad + F_C(t)\Gamma_C^{\mu\nu}(t)\big]u_\nu(\mathbf{p}_\Delta),\end{aligned} \tag{A.2}$$

where $t = (p'_N - p_\Delta)^2$ and magnetic $\Gamma_M^{\mu\beta}(t)$, electric $\Gamma_E^{\mu\beta}(t)$, and charged $\Gamma_C^{\mu\beta}(t)$ Lorentz-invariant combination are defined as follows:

$$\begin{aligned}\Gamma_M^{\mu\nu}(t) = &-\frac{3(m_N + m_\Delta)}{2m_N[(m_N + m_\Delta)^2 - t]}\epsilon^{\mu\nu\alpha\sigma} \\ &\times (p'_N + p_\Delta)_\alpha (p_\Delta - p'_N)_\sigma\end{aligned} \tag{A.3a}$$

$$\begin{aligned}\Gamma_E^{\mu\nu}(t) = &-\Gamma_M^{\mu\nu}(t) \\ &- \gamma_5 \frac{3i(m_N + m_\Delta)}{m_N[(m_N + m_\Delta)^2 - t][(m_N - m_\Delta)^2 - t]} \\ &\times \epsilon^{\mu\lambda\alpha\beta}(p'_N + p_\Delta)_\alpha (p_\Delta - p'_N)_\beta \epsilon_\lambda^{\nu\gamma\delta} \\ &\times p_{\Delta\gamma}(p_\Delta - p'_N)_\delta\end{aligned} \tag{A.3b}$$

$$\Gamma_C^{\mu\nu}(t) = -\gamma_5 \frac{3i(m_N + m_\Delta)(p_\Delta - p'_N)^\mu\left[t(p'_N + p_\Delta)^\nu - (p_\Delta - p'_N)^\nu\left(m_\Delta^2 - m_N^2\right)\right]}{2m_N[(m_N + m_\Delta)^2 - t][(m_N - m_\Delta)^2 - t]}. \tag{A.3c}$$

Charge form factor $\Gamma_C^{\mu\nu}(t)$ contributes in the calculation with the vertex functions. But in the tree approximation, where the four-vector $q^\mu = (p_\Delta - p'_N)^\mu$ is replaced with the real photon four-momentum $q^2 = 0$, contributions of $\Gamma_C^{\mu\nu}(t)$ disappears.

For the electric, magnetic, and charge formfactors we take the same cut-off function $f(t)$ as for the γ-proton vertex function

$$\begin{aligned}&F_M(t) = F_M(0)f(t); \quad F_E(t) = F_E(0)f(t); \\ &F_C(t) = F_C(0)f(t),\end{aligned} \tag{A.4}$$

where $F_M(0) = 3.2$ [40], $F_E(0) = 0.025 F_M(0)$ [42], and $F_E(0) = (m_\Delta - m_N)/2m_\Delta F_C(0)$ [31]. For our numerical calculation most sufficient is the magnetic part of Eq. (A2). The recent overview of the unified $N^* - N\gamma$ vertex functions is given in Ref. [41].

The $\pi N - \Delta$ vertex functions are defined in the standard way

$$\langle \mathbf{p}'_N | j_\pi(0) | \mathbf{P}_\Delta \rangle = \overline{u}(\mathbf{p}'_N) g_\Delta[(p'_N - P_\Delta)^2](p'_N - P_\Delta)_\sigma u^\sigma(\mathbf{P}_\Delta),$$

where the vertex function $g_\Delta[(p'_N - P_\Delta)^2]$ in the model A $\pi N - \Delta$ is $g(\mathbf{p})$ [Eq. (28)], in model B it coincides with the coupling constant [Eq. (30)] and in model C $\pi N - \Delta$ vertex function is $h(\mathbf{p})$ [Eq. (32)].

The $\gamma\Delta' - \Delta$ vertex functions are the same as in our previous article [2]. In this case $Q = P'_\Delta - P_\Delta$ and $R = P'_\Delta + P_\Delta$ and the $\gamma\Delta' - \Delta$ vertex function is as follows:

$$\langle \mathbf{P}'_\Delta | J_\mu(0) | \mathbf{P}_\Delta \rangle = \overline{u}^\sigma(\mathbf{P}'_\Delta) V_{\sigma\mu\rho}(\mathbf{P}'_\Delta, \mathbf{P}_\Delta) u^\rho(\mathbf{P}_\Delta), \tag{A.5}$$

where

$$\begin{aligned}V_{\sigma\mu\rho}(\mathbf{P}'_\Delta, \mathbf{P}_\Delta) = &\, g_{\rho\sigma}\left[\boldsymbol{F}_1(Q^2)\gamma_\mu + \frac{F_2(Q^2)}{2M_\Delta}R_\mu\right] + Q_\sigma Q_\rho \\ &\times \left[\frac{F_3(Q^2)}{M_\Delta^2}\gamma_\mu + \frac{F_4(Q^2)}{2M_\Delta^3}R_\mu\right].\end{aligned} \tag{A.6}$$

The form factors $F_i(Q^2)$ are simply connected with the charge monopole $G_{C0}(Q^2)$, the magnetic dipole $G_{M1}(Q^2)$, the electric quadrupole $G_{E2}(Q^2)$, and the magnetic octupole $G_{M3}(Q^2)$ form factors of the Δ^+ resonance. In the low-energy region we can neglect the terms $\sim Q^2/4M_\Delta^2$, and we keep only terms $\sim 1/M_\Delta$. Then the previous formula can be rewritten in a similar form as the γ-proton vertex function:

$$V_{\sigma\mu\rho}(\mathbf{P}'_\Delta, \mathbf{P}_\Delta) = g_{\rho\sigma} G_{C0}(Q^2)\frac{R_\mu}{2M_\Delta} + i g_{\rho\sigma}\frac{G_{M1}(Q^2)}{2M_\Delta}\sigma_{\mu\beta}Q^\beta. \tag{A.7}$$

In our case of soft photon emission we have approximated the form factors in Eq. (A7) with their pseudothreshold values $G_{C0}(Q^2) \to G_{C0}(t_{\text{ptr}} = 1$ and $G_{M1}(Q^2) \to G_{M1}(t_{\text{ptr}}) = \mu_{\Delta^+}$, where $t_{\text{ptr}} = (m_\Delta - m_N)^2$, and μ_{Δ^+} denotes the magnetic moment of the Δ^+ resonance and it is simply connected with the k_{Δ^+} anomalous magnetic moment of Δ^+ $\mu_{\Delta^+} = (1 + k_{\Delta^+})/2m_\Delta$.

The $V \equiv \rho, \omega$-meson-nucleon vertex functions in Eq. (2.11) have the following form:

$$\langle \mathbf{p}'_N | j_\mu^V(0) | \mathbf{p}_N \rangle = \overline{u}(\mathbf{p}'_N)\left[\gamma_\mu F_1^V(t) + i\frac{k_V}{2m_N}\sigma_{\mu\nu}(p'_N - p_N)^\nu F_2^V(t)\right]u(\mathbf{p}_N), \tag{A.8}$$

where $k_\omega = 0$ and $k_\rho = 3.7$. Form factors $F_1^V(t)$ are replaced with their threshold values $F_1^V(t) \Longrightarrow g_{VNN}$ and $g_{\omega NN} = 3 \times g_{\rho NN} = 15$ [43]. And for the $\rho(\omega)$ decay constant we have taken the value $g_{\omega\gamma\pi} = 3 \times g_{\rho\gamma\pi} = 0.374$ [25,44].

The π^o decay vertex function in Figs. 10(k), and 10(I) is taken in the standard form on the tree approximation [37,7]

$$\Gamma^{\mu\nu}_{\gamma'-\pi^o\gamma} \sim \int d^4x \langle 0 | T[j^\mu(x) j^\nu(0)] | \mathbf{p}_\pi = \mathbf{k}_\gamma - \mathbf{k}_{\gamma'} \rangle e^{ik_{\gamma'}x} \approx -i\frac{0.035}{m_\pi}\epsilon^{\mu\nu\alpha\beta}k_{\gamma_\alpha}k_{\gamma'\beta}. \tag{A.9}$$

[1] L. A. Kondratyuk and L. A. Ponomarev, Sov. J. Nucl. Phys. **7**, 82 (1968).
[2] A. I. Machavariani, Amand Faessler, and A. J. Buchmann, Nucl. Phys. **A646**, 231 (1999); Nucl. Phys. **A686**, 601 (2001).
[3] D. Drechsel, M. Vanderhaeghen, M. M. Giannini, and E. Santopinto, Phys. Lett. **B484**, 236 (2000).
[4] D. Drechsel and M. Vanderhaeghen, Phys. Rev. C **64**, 065202 (2001).
[5] M. Kotulla *et al.*, Phys. Rev. Lett. **89**, 272001 (2002).
[6] R. Beck, B. Nefkens *et al.*, Letter of Intent, MAMI (2001).
[7] H. Garcilazo and T. Mizutani, *πNN Systems* (World Scientific, Singapore 1990).
[8] V. Pascalutsa and O. Scholten, Nucl. Phys. **A591**, 658 (1995).
[9] A. D. Lahiff and I. R. Afnan, Phys. Rev. C **66**, 044001 (2002); **60**, 0236008 (1999).
[10] A. I. Machavariani and Amand Faessler, Ann. Phys. **309**, 49 (2004).
[11] J. D. Bjorken and S. D. Drell, *Relativistic Quantum Fields* (McGraw-Hill, New York, 1965).
[12] C. Itzykson and C. Zuber, *Quantum Field theory* (McGraw-Hill, New York, 1980).
[13] V. De Alfaro, S. Fubini, G. Furlan, and C. Rosseti, *Currents in Hadron Physics* (North-Holland, Amsterdam, 1973).
[14] M. K. Banerjee and J. B. Cammarata, Phys. Rev. C **17**, 1125 (1978).
[15] A. I. Machavariani, Fiz. Elem. Chastits At. Yadra **24**, 731 (1993).
[16] A. I. Machavariani and A. G. Rusetsky, Nucl. Phys. **A515**, 621 (1990).
[17] A. I. Machavariani, A. J. Buchmann, Amand Faessler, and G. A. Emelyanenko, Ann. Phys. **253**, 149 (1997).
[18] P. van Nieuwenhuizen, Phys. Rep. **68**, 189 (1981).
[19] H. T. Williams, Phys. Rev. C **31**, 2297 (1985).
[20] M. Benmerrouche, R. M. Davidson, and N. C. Mukhopadhyay, Phys. Rev. C **39**, 2339 (1989) and references therein.
[21] S. Gasiorowicz, *Elementary Particle Physics* (John Wiley & Sons, New York, London, Sydney, 1966).
[22] M. El Amiri, G. Lopez Castro, and J. Pestiau, Nucl. Phys. **A543**, 673 (1992) and references therein; G. Lopez Castro and A. Mariano, nucl-th/0010045.
[23] R. M. Davidson, N. C. Mukhopadhyay, and R. S. Wittman, Phys. Rev. D **43**, 71 (1991) and references therein.
[24] A. I. Machavariani, Few-Body Phys. **14**, 59 (1993).
[25] S. Nozawa, B. Blankleider, and T.-S. H. Lee, Nucl. Phys. **A513**, 459 (1990).
[26] J. V. Boss and J. H. Koch, Nucl. Phys. **A563**, 539 (1993).
[27] F. Gross and Y. Surya, Phys. Rev. C **53**, 2422 (1996).
[28] S. Wang and M. K. Banerjee, Phys. Rev. C **54**, 2883 (1996).
[29] K. Ohta, Phys. Rev. C **40**, 1335 (1989).
[30] H. Haberzettl, Phys. Rev. C **62**, 034605 (2000); H. Haberzettl, C. Bennhold, and T. Mart, Acta Phys. Pol. B **31**, 2387 (2000).
[31] H. F. Jones and M. D. Scadron, Ann. Phys. **81**, 1 (1973).
[32] L. Heller, S. Kumano, J. C. Martinez, and E. J. Moniz, Phys. Rev. C **35**, 718 (1987).
[33] R. A. Arndt, W. J. Briscoe, I. I. Strakovsky, and R. L. Workman, Phys. Rev. C **66**, 055213 (2002).
[34] D. E. Groom *et al.* (PDG), Eur. J. Phys. C **15**, 1 (2000).
[35] E. L. Hallin *et al.*, Phys. Rev. C **48**, 1497 (1993).
[36] H. Genzel *et al.*, Z. Phys. A **279**, 399 (1976).
[37] T. P. Cheng and Ling-Fong Li, *Gauge Theory of Elementary Particle Physics* (Oxford, Clarendon Press, Oxford, 1984).
[38] W. E. Fischer and P. Minkowski, Nucl. Phys. **B36**, 519 (1972).
[39] M. M. Giannini, Rep. Prog. Phys. **54**, 483 (1991).
[40] D. Drechsel, O. Hansen, S. Kamalov, and L. Tiator, Nucl. Phys. **A645**, 145 (1999).
[41] M. I. Krivoruchenko, B. V. Martemyanov, Amand Faessler, and C. Fuchs, Ann. Phys. (NY) **296**, 299 (2002).
[42] R. Beck *et al.*, Phys. Rev. C **61**, 035204 (2000).
[43] M. Guidal, J. M. Laget, and M. Vanderhaeghen, Nucl. Phys. **A627**, 645 (1997).
[44] Amand Faessler, C. Fuchs, and M. I. Krivoruchenko, Phys. Rev. C **61**, 035206 (2000).
[45] R. A. Arndt, J. M. Ford, and L. D. Roper, Phys. Rev. D **32**, 1085 (1985).
[46] W. T. Chiang, M. Vanderhaeghen, S. N. Yang, and D. Drechsel, Phys. Rev. C **71**, 015204 (2005).
[47] V. Pascalutsa and M. Vanderhaeghen, Phys. Rev. Lett. **94**, 102003 (2005).